A flexible device to produce a gas stream with precisely controlled water vapour mixing ratio and isotope composition based on microdrop dispensing technology

Harald Sodemann[1,2], Alena Dekhtyareva[1,2], Alvaro Fernandez[2,3,4], Andrew Seidl[1,2], and Jenny Maccali[2,3,5]

[1]Geophysical Institute, University of Bergen, Norway
[2]Bjerknes Centre for Climate Research, Bergen Norway
[3]Department of Earth Sciences, University of Bergen, Norway
[4]Andalusian Institute of Earth Science, CSIC-University of Granda, Spain
[5]SFF Centre for Early Sapiens Behaviour (SapienCE), University of Bergen, Norway

Correspondence: Harald Sodemann (harald.sodemann@uib.no)

Abstract. Here we describe a versatile device to produce a ~~flow of air-vapour mixture with controlled humidity and~~ gas stream with precisely controlled water vapour mixing ratio and stable water isotope composition based on microdrop dispensing technology. To produce a moist air stream, the microdrop dispensing technology ejects micrometer-size water droplets that completely evaporate into a stream of carrier gas heated to 60 deg C. By precisely controlling the contribution of water standards from two dispenser heads into a carrier gas stream, the device allows to set the air-vapour stream to any isotope ratio between two end member waters. We show that Allan deviation of the water vapour mixing ratio is 10 ppmv over more than 24 h, and reaches 0.004 ‰ for δ^{18}O and 0.02 ‰ for δ^2H for a flow rate of 40 sccm. Tests with flow rates from 40–250 sccm shows an increase of the Allan deviation with higher flow rates. Tests with mixing standard water from two dispenser heads shows a linear mixing across a range of water vapour mixing ratios from 1'000 to 20'000 ppmv. In addition to presenting the design and several performance characteristics of the new system, we describe two application examples. First, we ~~utilize~~ utilise the device to determine ~~a common artifact of vapour isotope analyzers, known as the~~ the water vapour mixing ratio – isotope ratio dependency, a common artefact of water vapour isotope spectrometers. Second, we ~~utilize~~ utilise the device to provide a constant background stream of ~~humid~~ moist air for fluid inclusion water isotope analysis in calcite samples from stalagmites. The observed flexibility and precision of the device ~~underpints~~ underpins its usefulness and potential for a wide range of applications in atmospheric water vapour isotope ~~measurement applications. Future improvements~~ measurements. Future developments could focus on reducing the number of manual interventions ~~and improved control at high flow rates~~ needed to clear dispenser heads from gas bubbles, and the provision of a water vapour stream at flow rates of up to several liters per minute.

1 Introduction

The composition of stable water isotopes in ocean and surface waters, land ice, and precipitation has long been used to extract valuable information about the climate system (Horita et al., 2008; Galewsky et al., 2016). Since the advent of instruments based on Cavity-Ring Down Spectroscopy (CRDS) for water isotope analysis (Kerstel et al., 2006; Lee et al., 2005; Gupta et al., 2009), water vapour can be measured continuously at a time scale of seconds, providing for example insight into the details of weather systems (e.g., Graf et al., 2019; Thurnherr et al., 2020). To match the precision and accuracy of Isotope-Ratio Mass Spectrometry (IRMS), laser-based isotope analysers need frequent calibration of the raw data to account for instrumental drift, and for the characterisation of spectroscopic baseline effects (Sturm and Knohl, 2010; Aemisegger et al., 2012). Currently, variability of the gas stream produced by the calibration system, both in terms of mixing ratio and isotope composition, together with inlet and instrument characteristics, are important contributors to the total uncertainty of atmospheric water vapour isotope measurements. Separating different contributions of uncertainty is in particular critical at low humidities, such as for airborne measurements (Sodemann et al., 2017) and in cold environments (Casado et al., 2016; Seidl et al., 2023). Correction functions for spectroscopic effects causing a dependency on both water vapour mixing ratio and isotope composition require a detailed characterisation of each analyser (e.g., Weng et al., 2020; Thurnherr et al. . The necessary, precisely controlled gas stream over sufficiently long averaging times requires an external vaporisation device with flexibility in terms of mixing ratio and isotope composition, and flow rates.

The characteristics and properties of such an external vaporisation device are critical to obtain accurate and precise measurements of the water vapour isotope composition. A range of devices with distinct designs have so far been used to generate a vapour stream for instrument characterisation and calibration. The bubbler design consists of a dry air stream that is percolated through a sufficiently large water reservoir at a defined temperature. The emanating water vapour has then an isotope composition in isotopic equilibrium with the liquid for the given temperature (e.g., St Clair et al., 2008). Despite its overall simplicity, there are several drawbacks with bubbler designs. First, precise temperature control is required to predict the isotope composition of the water vapour from equilibrium fractionation. Additionally, a reservoir of up to several liters of water may be needed to limit the impact of drift from the changing isotope composition in the liquid over time. Depending on the measurement platform and ambient conditions, handling of such amounts of liquid may be a hindrance during field deployments.

Another design concept to circumvent complications from isotope fractionation involves the complete evaporation of liquid water into a heated cavity. Such systems are for example commonly used for liquid sample analysis, where an autosampler injects about 2 μl of water into a cavity heated to 110 °C (e.g., van Geldern and Barth, 2012). Such systems only produce

55   a vapour stream of ~~a few minutes duration~~about 10 min, which is sufficient for liquid sample analysis, but not sufficient for longer-term instrument characterisations. Another design that allows for generation of a continuous vapour stream with complete evaporation is ~~based on a nebulizer head is~~ the water vapour isotope standard source (WVISS, Los Gatos Research, USA) using droplets emanating from a nebulizer head. The WVISS allows for production of a vapour stream over several hours for one standard at a time. In addition to manual intervention for changing standards, the system requires external modifications

60   to reach lower mixing ratios, and the achieved precision of the ~~vapour signal~~ water vapour mixing ratio can be a limitation for some applications (Aemisegger et al., 2012).

A further design concept ~~is to continuously inject~~ involves continuously injecting a small amount of standard water into a heated cavity by means of thin needles, such as used in the Standard Delivery Module (SDM, Picarro Inc, Sunnyvale, USA). Built as an external module added to the liquid water analysis setup of these ~~analyzers~~analysers, the SDM provides a vapour

65   stream at a typical flow of 35 sccm, supplied from water standard reservoirs by two syringe pumps. ~~The~~ While overall a reliable field calibration device, the mechanically operated syringe pumps ~~are~~ can be prone to failure of moving parts, and air bubbles in the lines can lead to strong oscillations in the mixing ratio, requiring manual intervention. Both can be important limitations for calibration in remotely-operated measurement setups (Bonne et al., 2014). A further design for water vapour generation with complete evaporation that has been used for example in providing a constant background humidity in fluid inclusion

70   analysis involves, and a peristaltic pump that delivers a water droplets into an N_2 gas stream heated to 140 °C (Affolter et al., 2014). A similar design has been used in the continuous analysis of water from ice cores on a melting bed, where the liquid is provided through a capillary to a heated oven (Gkinis et al., 2010) or from a circular nebuliser that produces a spray of 1.5 μm-size droplets (Jones et al., 2017). Both designs have ~~only limited possibility~~ been operated over extended time ranges (e.g., Bonne et al., 2019), but have not been constructed for flexibility, such as to regulate the mixing ratio of water vapour in

75   the ~~airflow, but have been operated over extended time ranges (Bonne et al., 2019)~~gas flow over a wide range.

~~A~~ The precise control of mixing ratio is in particular important for the provision of a water vapour stream background humidity in fluid inclusion analysis. The principle of fluid inclusion analysis relies on voids within the carbonate matrix of stalagmites that regularly preserve remnants of cave drip waters. Since these waters are the relics of past precipitation, their oxygen and hydrogen isotope compositions can be used to reconstruct past changes in cave temperature (e.g., McGarry et al., 2004; Meckler

80   and changes in the amount and/or source of precipitation (Fleitmann et al., 2003). Due to the small size of inclusions (<100 μm) and the low amount of water that is commonly present in stalagmites (0.05 to 0.5 weight%; Affolter et al. (2014)), isotope measurements are made on the water that is released when large aliquots (>50 mg) of carbonate are crushed in a heated apparatus. Due to the small water amounts, analysis of fluid inclusions in stalagmites requires a background vapour stream with precisely known isotope composition and mixing ratio as carrier gas. This known background enables to separate the

85   superimposed $\delta^{18}O$ and δ^2H signals of the water released from calcite cavities during the crushing.

Another design concept with both, complete evaporation of standard water and fine-grained control of the mixing ratio is based on the ~~dispension~~ dispensing of micrometer-size droplets (St Clair et al., 2008). Microdrop systems are essentially ink jet printer heads that eject droplets from a glass capillary at a defined size by means of piezoelectric stimulation. Thereby, the head is filled or emptied by pressure applied to the head space of the reservoir. During dispensing of droplets, the liquid is supplied to the printer head by capillary forces. The particular advantages of a microdrop system in the context of vapour stream generation is the precise control of the amount of water released from the dispenser head by modification of voltage and frequency (Iannone et al., 2009). Release of individual water droplets at a defined size enables fast and complete evaporation without fractionation artefacts. Sayres et al. (2009) applied a bubbler and a microdrop system with a high flow rate of dry gas (100 slm) to achieve a stable flow at low humidity (<200 ppmv) needed for calibration of cavity-based absorption instrument used for upper troposphere and lower stratosphere measurements. Sturm and Knohl (2010) built a prototype water vapour generator based on microdrop technology, that required manual change of standards, but the ~~technology~~ design has not been developed further for water vapour isotope analyses since. Therefore, there is currently no single system available that in ~~combination provides~~ a flexible way provides the combination of a precise stream of water vapour across a range of ~~mixing ratios, flow rates, and different stable isotope compositions~~ water vapour mixing ratios and isotope compositions as well as operation at various flow rates between 50 and 250 sccm.

Here we present a new, flexible and versatile calibration system for CRDS vapour isotope ~~analyzers~~ analysers based on microdrop dispensing technology, which allows to produce a precise vapour stream over a range of mixing ratios and flow rates. As a key innovation, we use two dispensing heads simultaneously, providing to our knowledge the first system that allows to generate a vapour stream with any isotope composition along the mixing line of two standards. Due to its flexibility, the device is suitable for a range of applications, including instrument characterisation, calibration of water vapour isotope measurements, and as a component in specific ~~laboratory applications~~ analytical setups, such as a crushing line for fluid inclusion isotope analysis in cave deposits (Affolter et al., 2014). In addition to presenting the design and performance characteristics of the new system, we describe here two different application examples of increasing complexity, namely the ~~characterization~~ characterisation of the mixing ratio – isotope ratio dependency of CRDS analysers, and the provision of background humidity for stalagmite fluid inclusion isotope analysis.

2 Application requirements, design objectives, and specifications

~~We designed the device for vapour generation in a way that would allow for a wider range of~~ Our primary design objective is to create a single, highly flexible device for the generation of a water vapour isotope stream that can be used in a variety of different applications with CRDS ~~analyzers than possible with any single currently available device. Such applications include~~ analysers. Application (i) ~~providing a background humidity~~ is to provide a constant background humidity with precisely controlled mixing ratio x and isotope composition in an analytical setup, specifically for fluid inclusion water isotope analysis. In this application, a vapour stream with precise mixing ratio (SD(30 min)<20 ppmv) at a set isotope composition should be provided for several hours to days. Application (ii) ~~Providing~~ is to provide a vapour stream for calibration with flow rates

4

varying between 35 and 250 sccm. This range of flow rates is required to produce the vapour stream required by analysers that run in different flow configurations, such as the standard low-flow configuration of Picarro analysers at 35 sccm, and the flux configuration with flow rates of about 150 sccm for aircraft measurements (Sodemann et al., 2017). At even larger flow of about 300 sccm through the cavity of the CRDS analyzer, flow rate limitations of calibration systems emerge as an important challenge (Thurnherr et al., 2020; Bailey et al., 2023). Even larger flow rates that would also allow to characterise the response times of entire inlet lines with additional flush pumps used in semi-permanent installations for water isotope analysis (e.g., Steen-Larsen et al., 2013; Bonne et al., 2014; Galewsky et al., 2016) would require downstream dilution with a dry carrier gas. We leave such larger flow rates to future applications. Application (iii) is to providing a wide range of isotope composition and mixing ratios for instrument characterisation. Characterisation of analysers in terms of their mixing ratio – isotope ratio dependency requires to independently step through mixing ratio and isotope composition (Weng et al., 2020). This is facilitated greatly by an on-line, adjustable mixing of the evaporated water between two end-member standards. To cover the typical ambient mixing ratios encountered in mid-to high latitudes from the surface to high-elevations, the range of mixing ratios should encompass at least 500 to 25000 ppmv. Furthermore, the entire system should be small, portable and robust enough to be part of a field installation, for example to set up in a 19 inch rack mount alongside the analyser on a ship or some measurement station.

These application requirements are in their combination not met by any single existing calibration system, and would require either a combination or modification to currently available systems. In particular the ability to set the isotope composition within a range is not available from current devices. For example, the SDM provides a more limited range of humidities (6'000–24'000 ppmv according to manufacturer specifications, even though lower humidities are possible), and at most 20 min of operation before a new cycle is started. The SDM is also limited to two standard waters and allows no easy exchange or mixing of different standards. To some degree, autosampler injections can be used to cover a range of isotope composition over different mixing ratios. However, this involves significant manual intervention and preparations, as different mixtures between water standards have to be prepared and analysed beforehand, and injection amounts have to be adjusted to obtain the desired range of water vapour mixing ratios in the vapour stream from the vapouriser module (Weng et al., 2020). The availability of one flexible device for several applications holds the promise of simplifying workflows, reducing error sources, and thus contribute to better data quality.

In summary, we chose the following specifications of the water vapour generator:

1. To produce a water vapour stream with mixing ratios between 500 and 25000 ppmv;

2. To provide gas flow rates of between 35 and 250 sccm;

3. To maintain a precicely regulated, drift-free water vapour stream over hours to days;

4. To allow for continuous mixing of the isotope composition between two end members;

5. To be portable enough to be setup with a CRDS analyser during a field installation.

3 Device components and setup

155 At its core, the calibration device consists of a vertical evaporation chamber where the vapour stream is generated (Fig. 1). The evaporation chamber is a custom modification of a 300 ml sample cylinder (Swagelok Inc., USA, Part No. 304L-HDF4-300-T) with 1/4 inch NPT threads on both ends ~~.~~ (Fig. A1). Two stainless steal tubes of 30 mm length and 10.1 mm inner diameter have been welded horizontally to the upper part of the evaporation chamber, facing each other at an angle of 60 °C and with a vertical offset of 10 mm ~~.~~ (Fig. A1b). The two tubes reach 3 mm into the interior of the chamber, and each holds a dispenser

160 head (Microdrop GmbH, Germany, Part Nr. ~~MK-K-130) .~~ MK-K-130-020) with an inner nozzle diameter of 50μm for liquids with a viscosity below 20 mPas. For our prototype design, we chose an unheated head with a medium-size nozzle, similar to the design of St Clair et al. (2008). Each dispenser head (DH) is connected to one 12 ml glass vial ~~mounted next to the evaporation chamber~~ that holds a liquid water standard and is mounted next to the evaporation chamber. Both DHs and the standard vials are connected to a control device that among other parameters controls the piezo-electric pulse voltage and duration, the pulse

165 frequency, and headspace pressure for both DHs. In order to reduce ~~the retention time~~ memory effects from the retention of water vapour ~~in the~~ on the walls inside the evaporation chamber, the assembly has been treated with a ~~hygrophobic~~ hydrophobic coating (SilcoNert, SilcoTec Inc., USA).

Dry air (synthetic air) or N_2 is introduced as a carrier gas at the lower end of the evaporation chamber ~~.~~ (Fig. 1). The carrier gas is heated during passage of 60 cm of 1/4 inch SS tubing that bends between two brass plates that are heated on the outside

170 by heat trace covered with metal mesh (Watcom Inc, USA). The heat trace wraps around both the gas heating assembly and the evaporation chamber, and is controlled to 60 °C. Temperatures near the DHs are monitored to remain below 60 °C to minimize evaporation of liquid directly from the DH, which could possibly interrupt the dispensing.

A manual valve provides either N_2 or dry air from a gas tank or other source to the calibration unit. At the entry into the heated tubing, a mass flow controller (GFC 17, Alborgh Inc, USA) regulates the flow rate electronically to a set value between 0

175 and 500 sccm. The experiments presented here were either performed with high-purity grade N_2 (Nitrogen 5.0, purity >99.999 %; Praxair Norge AS, x<5 ppmv), synthetic air (synthetic air 5.5, purity 99.9995 %; Praxair Norge AS, x<5 ppmv), or air sourced from a dry air generator with added drying cartridges (MT-400, VWR, USA, m<100 ppmv). Typically, the carrier gas was supplied with a pressure of <1 bar upstream of the mass flow controller.

At the upper outlet of the evaporation chamber, different applications tap the vapour stream from a 1/4 inch SS connection

180 with Swagelok compression fitting. Depending on the application, the vapour stream was directly provided to the CRDS ~~analyzer, or lead~~ analyser, or led into an analytical assembly upstream of the ~~analyzer~~ analyser. Typically, an open split allowed for excess vapour to be vented into the room, with a line leading to the Wave-Length Monitor (WLM) port of the Picarro ~~analyzers~~ analysers.
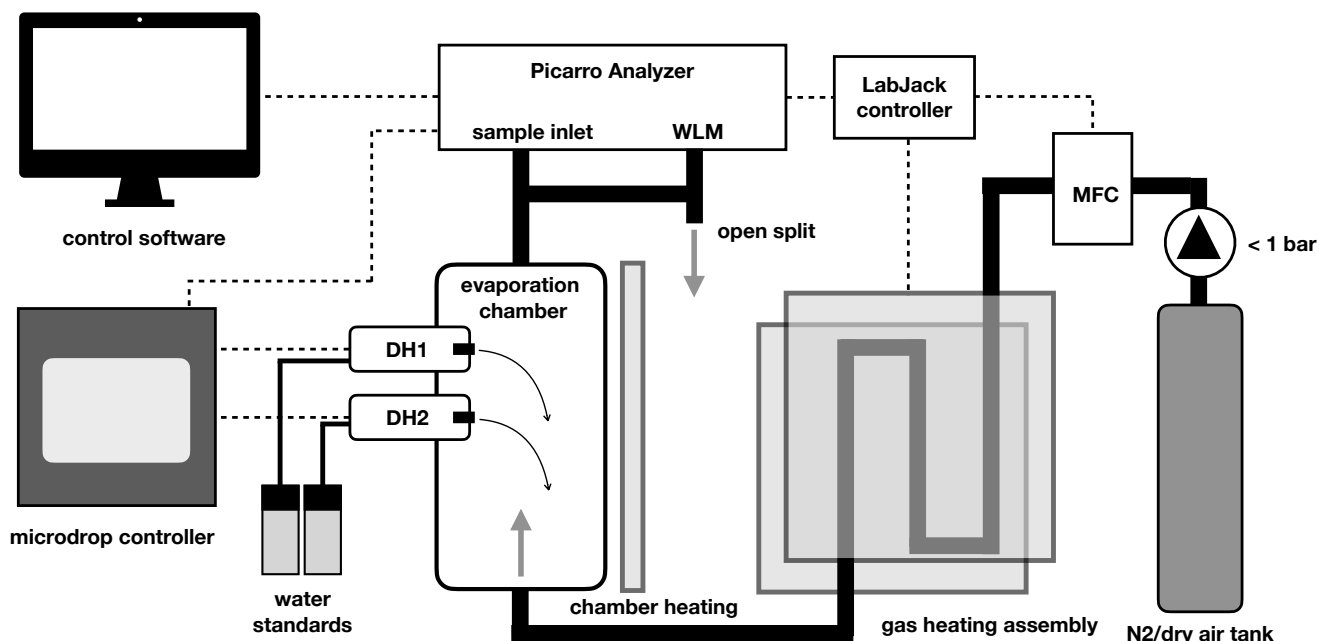
Figure 1. Schematic of the microdrop calibration device components. Thick black lines indicate tubing for gas flow. Dashed lines indicate electrical signal flow. Transparent grey areas denote heating elements. For further details see text.

A custom software written in python running on the Picarro ~~analyzer~~ analyser controls the flow rate of the mass-flow controller, the dispenser heads, and temperatures via a digital/analog interface (U12, LabJack Inc., USA). The software allows to manually fill, empty and modify settings for each DH, including ~~dispension~~ dispensing frequency, and to step through an automated sequence with a specific frequency at which each dispenser head injects droplets into the evaporation chamber.

4 Operating principle and procedures

The operating principle of the microdrop calibration device is based on the precisely controlled injection of liquid water droplets into the evaporation chamber. The number of droplets ~~of~~ at a specific size ejected into the evaporation chamber, which is flushed at a specific flow rate, results in a moist air stream with a water vapour and isotope ratio adjusted to the desired application.

7

Table 1. ~~Theoretical mixing~~ Mixing ratio and relative humidity at 60 °C of the air-vapour stream calculated for a typical and maximum range of ~~operating~~ dispensing parameters ~~for~~ resulting in a drop size of 70 μm. A typical range of mixing ratios through the L2130-i and L2140-i analyzers is between 200–40000 ppmv at a flow range of 35–300 sccm.

Frequency (Hz)	Carrier gas flow (sccm)	Mixing ratio (ppmv)	Relative humidity (%)
10	50	795	0.7
10	250	160	0.1
1000	50	79511	72.2
1000	250	15902	14.5

4.1 Droplet generation and droplet evaporation

The microdrop dispensing technology with the DHs used here allows to generate droplets with diameters ranging between 35.0 to 90.0 μm in diameter, depending on fluid properties (Table 2). The droplets can be ejected from the nozzle into the evaporation chamber with frequencies between 1 and 1500 Hz. As the droplets are ejected with about 2 ms^{-1} into the heated dry carrier gas flow, they rapidly evaporate before reaching the bottom of the evaporation chamber. The ~~drop~~ default factory calibration parameters can be modified to obtain different drop sizes. Thereby, the drop size range is more limited than the theoretically available range of drop sizes, as it depends on the nozzle diameter, fluid viscosity, and piezoelectric pulse voltage and duration parameters. We observed that, in line with manufacturer specifications, only at specific combinations of settings for the piezo-electric pulses (defined by voltage and duration) a single droplet, rather than a jet or sequence of drops was ejected. Higher voltages thereby tended to provide a droplet stream that operated over longer times before it could stop randomly, typically to the build-up of gas bubbles. The piezo-electric parameters needed to be determined for each DH in a relatively time-consuming procedure using a separate setup with a high-speed camera. According to manufacturer information, unless when operating at much higher voltages, the piezo-electric characteristics of each DH are thereby expected to be constant over time. Figure 2 gives examples for well-formed (panel a) and jet-like (panel b) droplet generation. Drop-like ejection is important for the linearity of the DH performance across frequencies and flow rates (Sec. 4.2). After suitable settings for the drop size had been found, the piezo-electric parameters were not modified further ~~until~~ . When a decrease of the DH performance or efficiency was observed, ~~typically after several months. The~~ this was in most cases due to the formation of gas bubbles which could be removed by repeated fill/empty cycles. The typical and theoretical limits for the specified rate of flow rates at the given ~~dropsize~~ drop size of about 70 μm are given in Table 1. With simultaneous operation of two DHs, a duplication of the mixing ratio is possible.

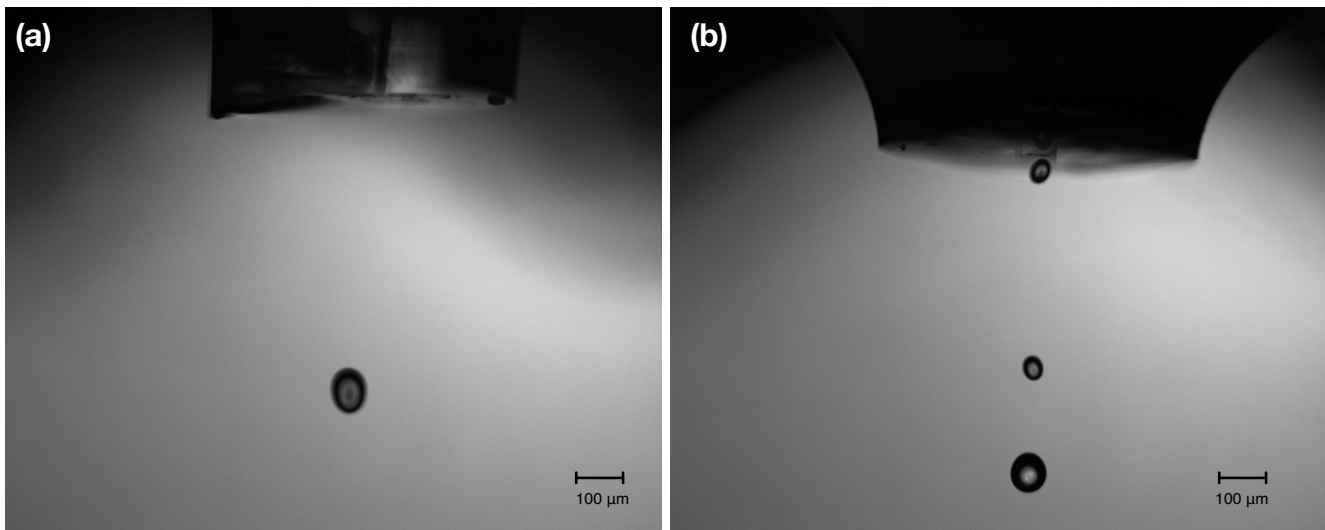## 4.2 Linearity and effective drop size

Figure 2. Pictures of microdrop dispenser heads in operation with ~~scale, well-formed and jet-like drop~~ different droplet examples. (a) Single drop emanating from DH with serial number 1016 at 85 V and 16 μs pulse width. (b) Jet-like drops emanating from DH with serial number 1015 with 85 V and a pulse width of 100 μs. Images have been obtained with a time-synchronized USB-b/w-camera with 10x objective (part #MD-O-539-USB, Microdrop GmbH, Germany).

Table 2. Performance characteristics and calibration parameters for 3 MK-K-130 DHs used in the microdrop device. As DH3 was purchased as a spare at a later time, we herein focus on results obtained with DH1 and DH2. Factory calibration parameters can be modified to obtain different drop sizes.

DH	1	2	3
Serial number	1015	1016	1032
Nozzle diameter	50 μm	50 μm	50 μm
Frequency range	1–1500 Hz	1–1000 Hz	1–1000 Hz
Tubing	10 cm PTFE	10 cm PTFE	11.5 cm PTFE
Calibration voltage	51 V	58 V	54 V
Calibration pulse length	39 μs	23 μs	26 μs
Calibration drop size	68 μm	74 μm	75 μm

Accurate control of the size of drops ejected from each DH is an important basis for mixing between water standards later on. As each dispensed drop adds a defined volume of water to the airstream, an ideal DH would provide a linear correspondence between the dispensing frequency and the mixing ratio of the resulting vapour stream. We can use ~~this relation between drop~~

~~size~~ the relation between flow rate, frequency and mixing ratio to compute the effective drop size of the DHs for a given voltage setting, pulse length, and run. To this end, we first calibrate the raw mixing ratio signal measured by the Picarro with a calibration curve obtained from a dewpoint hygrometer ~~.~~(Optisonde, GE Inc., USA). Then we compute the mass flux of the carrier gas at a given temperature, and obtain the effective drop size from the water mass contained in the air-gas mixture for a given frequency.

~~Figure 3shows the mixing ratio resulting for different DH operating frequencies, using dispersion~~ Day-to-day standard deviations of drop size are typically only a few micrometers (Fig. 3a, red and blue histogram), using dispensing parameters 82 V, ~~28~~18 μs for ~~both~~ DH1 and 82 V, 19 μs DH2. ~~Both DHs have different performance characteristics~~Median drop sizes are 64 μm for DH1 and 54.5 μm for DH2. The difference between the two DHs is a consequence of the DH geometry, which only allows to stably dispense single drops for a discrete sub-set of sizes that are particular for each head. Figure 3b shows the mixing ratio resulting for different dispensing frequencies. Very limited scatter is apparent for both heads that represents day-to-day variability. Due to the different drop sizes, both DHs have different efficiencies, quantified by the slope of a linear fit. DH1 (blue) has for the given settings an efficiency of ~~about 200~~207 ppmv Hz^{-1}, compared to ~~125~~130 ppmv Hz^{-1} for DH2 ~~. In addition, some scatter is apparent for both heads that represents day-to-day variability. Importantly, the~~ (blue). The results in Fig. 3a~~a~~ b are obtained for ~~non-ideal disperson~~ well-tuned dispensing settings, where ~~a jet rather than~~ discrete bubbles were ejected from both DHs ~~.~~(compare Fig. 2b). If the system is operated using dispersion parameters that lead to ~~single drops~~jets, the performance characteristics ~~improve~~ degrade markedly, both in terms of linearity ~~(Fig. 3b)~~ and day-to-day reproducibility ~~(Fig. ??). Day-to-day standard deviations of drop size are typically only a few micrometers (Fig. ??, red and blue histogram).~~ ~~Over the entire time period, the variability was substantially larger (Fig. ??, grey histograms). This result demonstantes the need to determine the effective drop size and a~~ not shown). Overall, this analysis demonstrates that once suitable dispensing parameters ~~repeatedly over time to control the~~ have been determined, the microdrop device produces a well-constrained linear relation between the amount of liquid released from a dispensing head ~~for~~at a given frequency and the water vapour mixing ratio in the air stream.

~~Histograms of droplet size computed from the dispensing parameters (a) for DH1 and (b) for DH2 with all dispersion parameters (grey shading, black median and standard deviation) and only with dispening parameters 82 V, 18 μs for DH1 (blue) and 82 V, 19 μs for DH2 (red).~~

4.3 Liquid water standard preparation

The water standards used here are secondary laboratory standards calibrated at FARLAB, University of Bergen on the VSMOW-SLAP scale with primary standard material provided by IAEA, according to their recommendations (IAEA, 2009). We used a depleted standard (GLW, -40.10±0.03 for δ^{18}O; -308.8±0.1 for δ^2H) and a standard close to local meteoric waters (DI2, -7.64±0.02 for δ^{18}O; -49.8±0.3 for δ^2H). Prior to filling DH reservoirs, the standard waters were filtered using a 0.2 μm PTFE filter (Part No. 514-0066, VWR, USA). This procedure is recommended by the manufacturer to prevent clogging of the DH capillary and PE tubing, and thus damage to the DHs. Furthermore, ~~to prevent the DH from arbitrarily stopping dispensing due to gas bubbles~~ gas bubbles forming in the capillary ~~, dissolved gas was removed~~ are a major factor that can lead to arbitrary
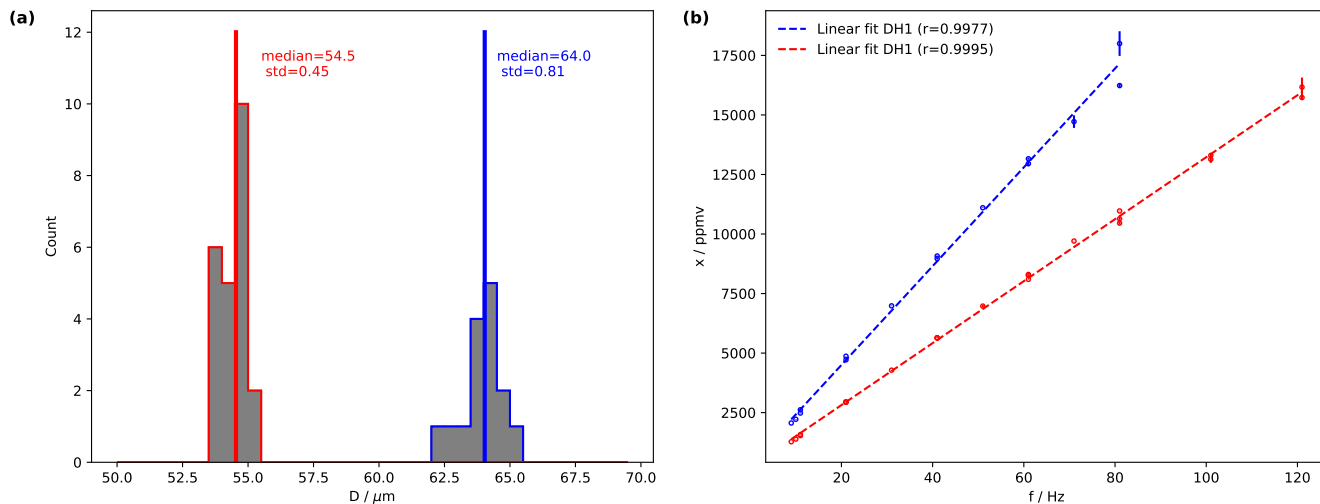
Figure 3. Performance of two dispenser heads at fixed droplet generation parameters and variable frequency. ~~Measurements have been performed on a Picarro L2140-i analyser (serial no. HKDS2038) (~~a) ~~with~~ Histograms of droplet size computed for DH1 from the dispensing parameters ~~82V~~82 V, ~~28~~18 μs ~~for both DH1~~ (blue) and ~~for~~ DH2 for 82 V, 19 μs (red) with median and standard deviation. Linearity of water vapour mixing ratio (~~b~~ppmv) versus dispensing frequency (Hz) for DH1 with dispensing parameters ~~82V~~82 V, 18 μs ~~for DH1~~ (ref) and ~~82V~~for DH2 with 82 V, 19 μs ~~for DH2~~(blue). Measurements have been performed on a Picarro L2140-i analyser (serial no. HKDS2038).

stopping of dispensing. Effective de-gassing is particularly important since our water standards are stored in stainless steel containers pressurised with Argon at about 1 bar. We initially removed dissolved gas from the liquid by suspension of the vials in an ultrasonic bath for about 15 min. After discussion with Microdrop GmbH, we found application of a vaccuum in a closed syringe dramatically increased effectiveness of the de-gassing, resulting in regularly uninterrupted dispensing of more than 255 24 h at a time.

4.4 Operating procedures

Before ~~producing a vapour stream~~starting to operate the microdrop device, the standards need to be filtered and degassed, filled into reservoirs, and the device heated to the operating temperature of 60 °C (typically <30 min) with gas flow enabled (>35 sccm). This heating time will allow the device to reach a residual background mixing ratio of well below 100 ppmv. 260 Thereafter, the standard operating procedures for the calibration device to produce a vapour stream include the following steps:

1. Remove DHs from evaporation chamber

2. Empty and fill DH with standard water using software control, wait for holding pressure to ~~stabilize~~ stabilise

3. Test DH operation by ejecting onto a lint-free piece of cloth, lit by a bright light source on a dark background at high ~~dispension~~ dispensing frequency (1000 Hz)

11

4. Stop dispensing and insert DH in evaporation chamber, attach and seal DH

5. Start dispensing at desired frequency from software.

These steps need to be followed at the start of a measurement sequence, but also each time when DH operation stops accidentally (Sturm and Knohl, 2010). Critical aspects during this normal operation sequence, and error sources leading to interruptions or poor calibration system performance are discussed in Sec. 8.

5 Device characteristics

This section presents typical results for the device characteristics regarding the linearity of the DH performance, stability of the calibration air stream, and ability of the system to generate mixtures of different standard waters at different flow rates.

5.1 Short-term stability

Stability of the water vapour mixing ratio and isotope composition of the calibration device are important in isotope analysis, and need to be quantified. In order to assess stability of the microdrop vapour device across a range of time scales for a continuous period of operation, we use the Allan deviation, which is given by the square root of the ~~Allen variance (e.g., Sturm and Knohl, 2010)~~Allan variance (Allan, 1966; Sturm and Knohl, 2010):

$$\sigma^2(\tau) = \frac{1}{2n} \sum_i^n \left(y_{~~i+1~~ i+1}(\tau) - y_i(\tau) \right)^2 \tag{1}$$

hereby, τ is the averaging time, y_i is the average value of measurements in an averaging interval i, and n is the number of averaging intervals for a given averaging time τ.

The minimum of the ~~Allen~~ Allan deviation indicates the optimal averaging time, where the highest measurement precision can be achieved. While measurement precision is primarily a property of the CRDS ~~analyzer~~analyser, the vapour stream needs to be sufficiently stable to enable ~~analyzer~~analyser characterisation. Thus, variability of the vapour stream needs to be minimal to identify instrument characteristics, rather than calibration system characteristics from the analysis of the ~~Allen~~ Allan variance. The ~~Allen~~ Allan deviation has been assessed from a constant operation of the microdrop device, dispensing at ~~65~~24 Hz with DH1 into a N$_2$ stream of ~~70~~40 sccm during about ~~4~~28 h, resulting in an average mixing ratio of about ~~18'400~~10'440 ppmv~~(Fig. 4).~~. For averaging times below 10 s, the ~~Allen~~ Allan deviation of the mixing ratio is less than ~~5~~2 ppmv, and remains below 10 ppmv for ~~up to 30 s average times .~~all remaining averaging times (Fig. 4, red line). The maximum variance of about ~~30~~10 ppmv is reached after ~~100~~400 s. We compare this to a measurement sequence obtained with the SDM and the same standard with daily calibrations during 25–29 March 2021. In total five calibration sequences have been combined to a 1:45 h time series for the assessment of the ~~Allen~~ Allan deviation of the same ~~analyzer~~analyser with an SDM (Fig. 4, black lines). ~~Notably,~~Thereby, we acknowledge that the SDM is not designed for mixing ratio ~~, the SDM has generally~~ stability, but for the stability of the isotopic signal. For mixing ratio, the SDM has a factor of ~~5~~10 or more lower
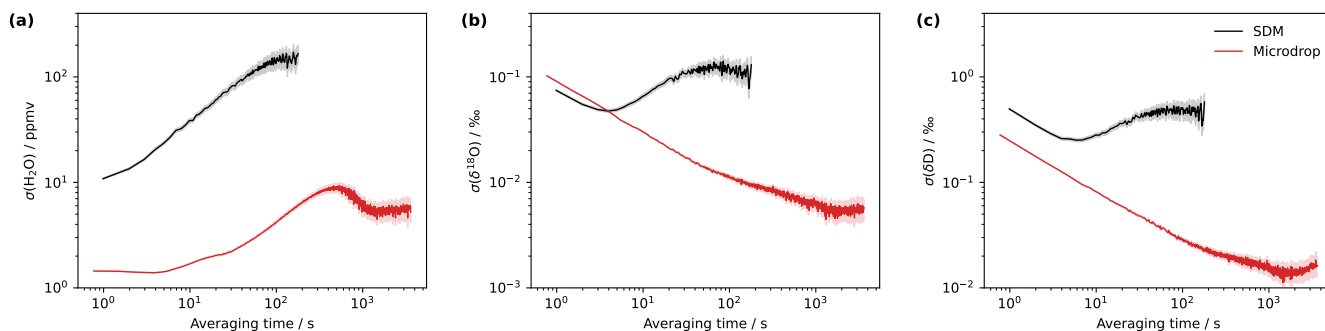
Figure 4. ~~Allen~~ Allan deviation for (a) mixing ratio (ppmv), (b) δ^{18}O (‰) and (c) δ^2H (‰) by the microdrop device (red) and an SDM (black) on ~~analyzer HIDS2254~~ analyser HKDS2039 with standard ~~DI2~~GLW. The microdrop measurements were performed in the laboratory on ~~08 March~~ 12–14 August 2023. The SDM measurements were combined from a set of shorter daily calibration ~~perids~~ periods obtained from 25–29 March 2021.

precision than the microdrop device, with an overall minimum of 10 ppmv. For δ^{18}O, the ~~Allen~~ Allan deviation with the SDM is initially lower than for the microdrop device, but reaches a minimum of only 0.05 ‰ after about 4 s, whereas the microdrop device provides the highest precision of ~~0.03~~0.004 ‰ after about ~~25~~1000 s (Fig. 4b). For δ^2H, the findings are similar, with a minimum in the Allan deviation for the SDM at 4 s with about 0.3 ‰, compared to below ~~0.2 after 300~~0.02 ‰ after 1000 s with the microdrop device (Fig. 4c). The results obtained for the microdrop device ~~appear in a~~ are in a very similar range as with a ~~capillay~~ capillary vapour generator obtained by Steig et al. (2014) and for the ~~WVIA generated Allan deviation~~ Allan deviation generated by WVIA in Aemisegger et al. (2012) for the same type of ~~analyzer, albeit these studies considered much longer measurement periods, and thus achieve a lower minimum at longer averaging times. We note here that the micodrop~~ analyser. From this analysis, we note that the microdrop device is able to provide a vapour stream with properties that allow to determine the precision of the ~~analyzer~~ analyser consistent with literature. The SDM vapour stream used here was substantially more noisy, and does not appear to be equally useful for ~~analyzer characterisation. It is therefore~~ analyser characterisation. These findings underline that it is important to consider the contribution of the vapour generation device when characterising the short-term stability of a CRDS water isotope ~~analyzer~~analyser, in particular for applications that require precise control of the mixing ratio, such as fluid inclusion analysis.

5.2 Long-term stability

Stable background water vapour mixing ratios and δ^{18}O and δ^2H values are particularly important for accurate and precise fluid inclusion data. We evaluated the long-term stability of the microdrop system as part of a crushing line setup (Sec. 7). From 16 analytical sessions with the crushing line over a period of 5 weeks, we obtain H_2O concentrations between 9550 and 13500 ppmv for 37 different occasions (Table A1). We selected a duration of 15 min to calculate short-term stability of each fluid inclusion sample peak measurement in that period (see Sec. 7). As a measure of long-term stability, we find an
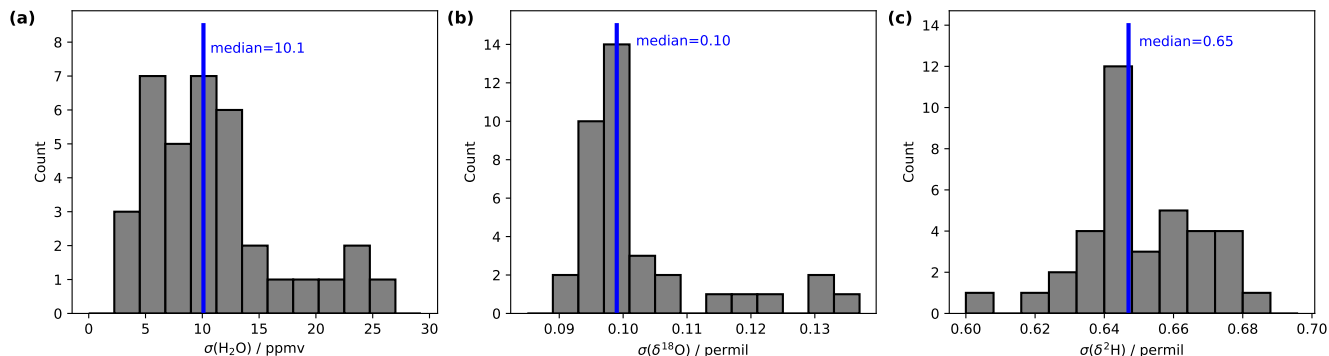
13

Figure 5. Long-term stability of the vapour stream assessed during a range of measurement days in Oct-Nov 2020. Histograms show standard deviations on (a) water vapour mixing ratios (ppmv), (b) δ^{18}O (‰) and (c) δ^2H (‰) values, calculated over 15 min long time intervals (n=37).

average standard deviation of 11.6±6.6 ppmv for water mixing ratio, 0.10±0.01 ‰ for δ^{18}O, and 0.65±0.02 ‰ for δ^2H values
315 on a 15 min time scale in this humidity range (Fig. 5). These standard deviations are much lower than typical sample peak heights during fluid inclusion measurements (see Sec. 7 and Fig. 13 below) as required for reliable fluid inclusion analysis (Affolter et al., 2014; Dassié et al., 2018; de Graaf et al., 2020). The long-term stability obtained here is also in a similar but slightly larger range as the short-term stability (Fig. 4). The larger variability on longer time scales can be induced by different factors in the analytical line setup and the microdrop device, including variation in ~~dispensor head performance~~ dispenser head
320 performance due to potential bubble formation, build-up of residual in the crusher line, ~~and other factors~~ among others (Sec. 7 and 8).

5.3 Variation of carrier gas flow rate

The currently used mass flow controller allows to regulate the flow rate in a range of 0–500 sccm. When using a Picarro L2140-i ~~analyzer, or similar,~~ analyser in low-flow mode, ~~at least 50~~about 40–50 sccm of gas flow are required to avoid leakage
325 of ambient air from the open split. Importantly, with ~~faster~~ larger gas flow, the residence time of the vapour stream in the microdrop device decreases, and ~~becomes potentially~~ flow can become turbulent in the evaporation chamber. Thus, ~~faster~~ higher flow rates can lead to better mixing conditions, and offset the ~~fall~~ falling of droplets to a larger degree. On the other hand, slight overpressure may build up in the evaporation chamber, which counteracts the operation of the DH. We therefore investigated the performance of the device in terms of the Allan deviation (Eq. 1) for water vapour and the isotope composition
330 at three different flow rates. To this end, DH1 was operated with laboratory standard DI2 for about 3-hour long segments with N$_2$ flow rates of 70, 140 and 250 sccm, and respective dispensing frequencies of 120, 210 and 350 Hz during 08–12 March 2022. The mixing ratio in all three setups was between 18'000 and 20'000 ppmv . The Allan deviation for 70 and 140 sccm is very similar for both mixing ratio (Fig. 6a) and the two isotope values (Fig. 6b,c). At averaging times of 30 s and longer, the Allan deviation becomes about 2 times larger for 140 sccm (black line) than 70 sccm (red line). At a flow rate of 250 sccm (blue
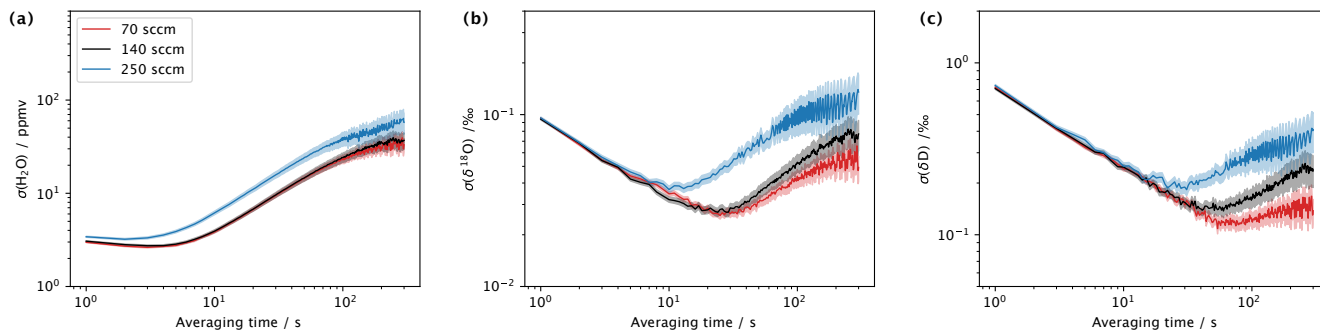
14

Figure 6. Comparison of Allan deviation for (a) water vapour mixing ratio (ppmv), (b) δ^{18}O (‰), and (c) δ^2H (‰) at flow rates of 70 sccm (red), 140 sccm (black), and 250 sccm (blue) obtained from a sequence of measurements at mixing ratios of 18'000-20'000 ppmv during March 2022.

335   line in Fig. 6), the Allan deviation is larger for the mixing ratio throughout the range of averaging times (Fig. 6a), while for both isotope species, the Allan deviation only increases for averaging times of more than 10 s. This indicates that the microdrop device can produce a usable vapour stream at flow rates of up to 250 sccm. However, the mixing ratio is more variable, and an additional mixing chamber may be required downstream to further stabilise the vapour stream.

5.4   Mixing of water from two dispenser heads

340   ~~With the presence of two DHs dispensing water standards that have large differences in isotopic composition~~Due to the two independently operated DHs, it is possible to produce a vapour stream that is freely mixed ~~from simultaneously operating two heads~~two water standards that have large differences in isotopic composition. We have tested the linearity of the mixing across a range of frequency settings using standards DI2 and GLW. Using frequency ratios $r = $ DH2/(DH1 + DH2) of 0.0, 0.2, 0.3, 0.4, 0.5, 0.6 and 1.0, we step through a range of frequencies for both dispenser heads. For example, to obtain a mixing ratio of

345   5000 ppmv at $r = 0.2$, we dispense with a frequency of 5 Hz from DH2 and 20 Hz from DH1 (ignoring sensor head efficiency for simplicity at this point). The ~~linearity of this mixing is provided over a range of mixing ratios~~ mixing between DHs is to first order linear (Fig. 7a). ~~Thereby,~~ In particular for lower mixing ratios, deviations become apparent (color shading). Both the efficiency of the dispenser heads ~~needs~~ (Sec. 4.2), and the combination of the frequency of each DH, which is an integer number in the current version of the control software, need to be taken into account for precisely regulating the mixture~~(Sec.~~

350   ~~4.2).~~. At lower humidity than 5000 ppmv,~~deviations from the linear mixing become apparent (Fig. 7b). These deviations are however not due to~~ some of the deviations are due to spectroscopic baseline effects. In the experiments presented here, the ~~changes in the dispensing frequency, but rather an effect of the mixing ratio – isotope ratio dependency (Weng et al., 2020). As in the results of Weng et al. (2020), obtained from liquid injections and SDM measurements, the humidity dependency varies with isotope ratio and isotope species at mixing ratios below about 5000 ppmv . This is for example seen when comparing~~

355   ~~the raw~~lowest RMSE between the predicted and actual isotope composition was obtained with mixing ratios of 20'000 ppmv
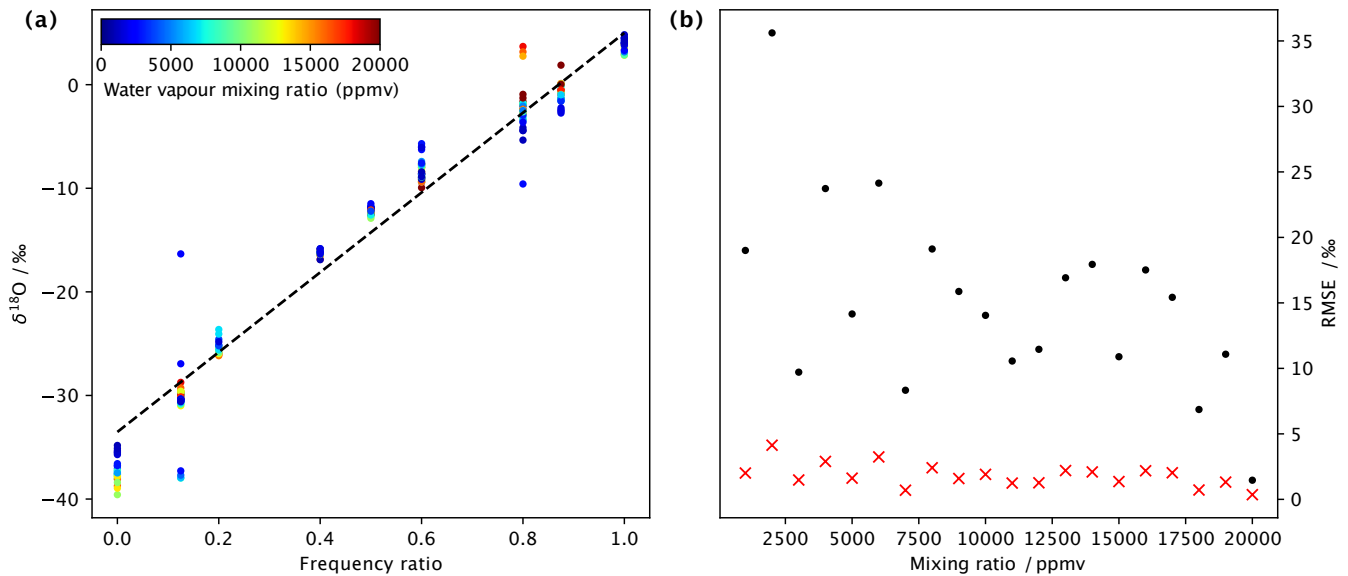
15

Figure 7. Stability of isotope standard mixing across range of humidities at an averaging time of 10 min. (a) Mixing line between two end members (laboratory standards DI2 and GLW) as a function of the ratio of dispensing frequency for $\delta^{18}O$ (‰) at different mixing ratios (ppmv, color shading). Dashed black line is a ~~1:1 reference line~~linear regression to all available data points. (b) Root-mean square error ~~of the observed mixing line~~ (‰?), calculated ~~using the reference line, as~~ from a ~~function of different mixing ratios~~ linear regression in comparison to the data points for $\delta^{18}O$ (red crosses) and δ^2H (black dots) mixing line for categories of different mixing ratio at a 1000 ppmv interval.

(Fig.7b), with 0.36 ‰ for $\delta^{18}O$ ~~signals bending downward for Mix000 and upward for Mix100 at below 5000 ppmv. By~~ (red crosses) and 1.46 ‰ for δ^2H (black dots). At lower humidity, the RMSE was typically around 1–2 ‰ for $\delta^{18}O$ and 10–15 ‰ for δ^2H. With corrections to the efficiency of the heads and more suitable combinations of dispensing frequency and gas flow, we expect that a more precise control of the mixing between end members can be achieved. Nonetheless, we conclude that by

360 varying the dispensing frequency at a fixed frequency ratio, and in addition changing the flow rate, a vapour stream with given isotope ratio can be produced over a wide range of mixing ratios. Thus, the microdrop vapour generator can be used to quantify ~~the mixing ratio – isotope ratio dependency for~~ for example spectroscopic baseline effects for nearly arbitrary positions in the mixing ratio – isotope ratio space (Sec. 6).

6   Application 1: Characterisation of the isotope composition-mixing ratio dependence of CRDS ~~analyzers~~analysers

365 We now present a first application example ~~where the~~ for the use of the microdrop vapour generator~~is directly connected to the analyzer~~. In this application example, ~~we~~ the device is directly connected to the input port of the analyser with an open split (Fig. 1). We then exploit the capability of the calibration system to ~~modify~~ independently vary both mixing ratio and isotope ratio, and thus obtain a detailed characterisation of the mixing ratio – isotope ratio dependency~~(Weng et al., 2020).~~

16

~~This measurement artefact results from the performance of Picarro L2130-i and L2140-i CRDS analysers being optimized for~~
~~liquid sample analysis at a water vapour mixing ratio of approximately 20000 ppmv. If the analyzer samples air or nitrogen~~ . As noted above, this dependency is a measurement artefact that results from spectroscopic effects, such as uncertainties from the spectral fitting and the correction of baseline effects (Sturm and Knohl, 2010). In particular at water vapour mixing ratios below about ~~5000-10000~~ 10000 ppmv, the raw measurements need to be corrected for this artefact. ~~Earlier studies detected this as~~ Early studies detected first a mixing ratio dependency (Lis et al., 2007; Sturm and Knohl, 2010; Steen-Larsen et al., 2013; Bastrikov et al., 2014). Based on a systematic investigation with different water standards, Weng et al. (2020) detected ~~an additional~~ in addition a systematic dependency on the isotope ratio~~. While they proposed that this mixing ratio – isotope ratio dependency has a spectroscopic origin, they confirm that the~~ , and proposed corresponding correction functions. The shape of this measurement artefact ~~is also specific for different instrument types and the used matrix~~ specific for each analyzer, and also the used carrier gas (Aemisegger et al., 2012; Bailey et al., 2015). As electronics and other components age, this dependency needs to be obtained at regular intervals to maintain high data quality for water vapour isotope measurements.

The correction procedure of Weng et al. (2020) allows to correct the uncalibrated isotope measurements for ~~this artefact~~ the combined water vapour mixing ratio and isotope ratio dependency, in particular for low mixing ratios. However, ~~two limitations have been identified in that study: (i) The characterization experiments with the above-mentioned vapour-generation techniques~~ the characterisation experiments are time consuming ~~, (ii)~~ with existing water vapour generators, require manual preparation and calibration of additional standard waters, and ~~(iii) are consequently~~ are thus usually based on a limited number of standards (5 in the case of Weng et al. (2020)). The microdrop calibration device presented here alleviates these difficulties by allowing to create an arbitrary mixture of standard waters at a specific isotope composition and mixing ratio, thereby providing the ~~isotope composition–mixing ratio~~ mixing ratio – isotope ratio dependency for a given ~~analyzer~~ analyser in high detail, specifically in regions of the mixing ratio – isotope ratio space where the artefact is particularly pronounced.

6.1 Experimental setup

The microdrop vapour generator was connected directly to the inlet of the Picarro analyser (L2130-i, Ser. No. ~~HIDS 2254~~ HIDS2254 or L2140-i, Ser. No. HKDS2038) with a stainless steel T-piece. Thereby, the overflow port was connected to the WLM Purge Port, secured by a check valve (Part Nr. SS-2C-1/3, Swagelok Inc, USA) to prevent leakage of ambient air into the ~~analyzer~~ analyser inlet line. To achieve the desired humidity, the DH frequency was stepped up and down within a range of typically 1 to 100 Hz, while the flow rate of the dry matrix gas was set to 70, 100, 200 and 300 sccm.

Mixtures of the end member standards were injected by altering the DH frequency ratio for each of the two heads. For example, a 50 % contribution of enriched standard from DH1 (raw δ^{18}O=2.6 ‰ and δ^2H=12.1 ‰ at approximately 20000 ppmv) and 50 % of depleted standard (raw δ^{18}O=-39.7 ‰ and δ^2H=-311.9 ‰ at approximately 20000 ppmv) from DH2 would result in an intermediate raw mixed signal (raw δ^{18}O=-16.0 ‰ and δ^2H=-130.5‰ at approximately 20000 ppmv), taking into account the efficiency of the two DHs (see Sec. 4.2). ~~The resulting mixture was named Mix50, given by the percent contribution of the enriched standard.~~

Each sequence typically covered a humidity range from about 20000 to 500 ppmv. An example for a typical humidity sequence during such a run ~~(Fig. 8) shows the~~ shows the end of an initial drying of the evaporation chamber to reach sufficiently low background mixing ratio ~~(between 13:30 and 13:35 down to~~ <100 ppmv ~~) with N$_2$ prior each calibration sequence~~(Fig. 8a, label A). Then, the ~~gas supply was switched to the synthetic air, and the~~ sequence starts by flushing the evaporation chamber with ~~a vapour mix of standards specific for this sequence~~ moist air at a frequency ratio of 0.6 at a maximum frequency of 50 Hz for 5 min until 13:40 (label B), followed by another drying sequence to remove some vapour remaining from the previous run together with the new vapour ~~. At the first calibration step , the frequency of 67 Hz was set for 6 s prior setting the desired~~ until 13:45 ~~Hz at the DH1. This alternating pattern was used for quickly transitioning between two different humidity levels. Similarly, when stepping down~~ (label C). Then, at 13:45, the first step starts dispensing from both DH at frequency ratio 0.6 (label D, blue dashed line). To allow for a more quick transition between different mixing ratio steps, the first seconds at the start of each step the target frequency have been exaggerated. For example, when going from 45 to 39 Hz ~~at the~~ with DH1, a 19 Hz frequency was used for ~~a brief initial period from 13:55 to 13:56~~ 6 s to provide a faster step down (Fig. 8, ~~before second step). The 60.0 s waiting time was set to adjust humidity before setting the desired frequency of 39 Hz. After the transitions~~label D). Then, the frequencies of both DHs were kept constant for 10 min, ~~leading to plateaus of mixing ratio and isotope ratio.The transition period of~~ providing flat segments of water vapour mixing ratio (Fig. 8a, label E) and isotope ratios (Fig. 8b,c). For the characterisation of the mixing ratio – isotope ratio dependency, the initial 5 min ~~between two concentrations was removed~~before further analysis. ~~The precision during remaining periods~~ of each segment were removed, while the following 5 mins were retained and averaged (Fig. 8, red segments)~~was~~. The precision of water vapour mixing ratio during the retained segments were typically 8.2 ppmv (median of one-sigma standard deviation ~~over a remaining~~ for retained 5 min ~~period), with a range of 0.4 to 1722.3 ppmv~~periods).

6.2 Obtaining an isotope composition-mixing ratio dependency correction for a CRDS ~~analyzer~~analyser

To obtain the isotope composition-mixing ratio dependence functions for the same CRDS ~~analyzer~~ analyser as in Weng et al. (2020) (L2130-i, Ser. No. HIDS2254), experiments with five different DH frequency ratios (100-80-60-40-20) covering the humidity range from 450 to 25000 ppmv have been conducted. Each experiment was repeated at least three times to obtain statistical significance of the measured results. Then, averages and standard deviation for each humidity step identified as ~~above were calculated~~as described below~~in Sec. 6.1 were calculated. After an arbitrary stop of one of the DHs manual intervention was required. In some cases, leakage of water vapour from the second, stopped dispenser head required filtering for outliers. Here, measurement points for which the isotopic composition differs from the expected value at 20000 ppmv by more than 20 % have been excluded as outliers. Furthermore, the points for the mixing ratio above 5000 ppmv for which the standard deviation of the δ^{18}O-value exceeded the 75th quantile of the standard deviation of δ^{18}O for all measurements have been removed. These outliers occurred due to strong variability in mixing ratio during the step or due to unstable functioning of one or both of the DHs, possibly due to formation of gas bubbles inside the DHs. ~~The remaining~~With more effective de-gassing of the standards, the number of stopped runs leading to outlier removal has been substantially reduced. The remaining 203 data points, ~~supplement by the measurements~~ supplemented by the measurement points of Weng et al. (2020), were then used to
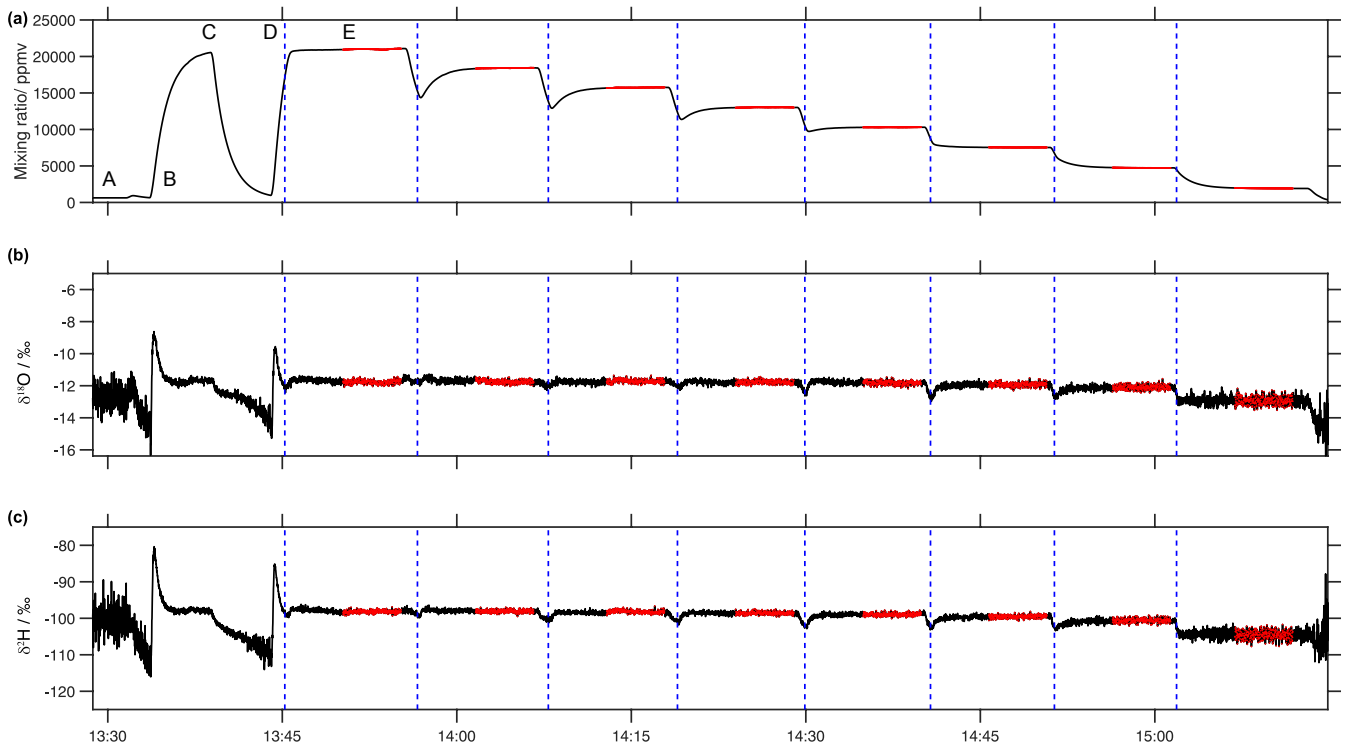
Figure 8. Typical sequence of (a) water vapour mixing ratio (ppmv), (b) $\delta^{18}O$ (‰) and (c) δ^2H (‰) during a calibration run on the ~~FARLAB~~ microdrop ~~evaporator~~device. Example depicts a run with Picarro ~~analyzer~~ analyser HKDS2038 ~~and~~ using synthetic air as a carrier gas, ~~standard~~ and a mixture ~~Mix060~~ of standards (60% DH1 and 40% DH2) on 04 June 2021, with 8 steps of 10 min duration (marked with dashed vertical blue lines) and 5 min stable period within each step (marked with red colour) used to calculate the average values and standard deviation of stable water isotopes and mixing ratio.

construct the mixing ratio – isotope ~~composition~~ ratio dependency correction (Fig. 9, blue points). As in previous studies, we use a reference value δ_{ref} at 20'000 ppmv to determine the deviation $\Delta\delta_{corr}$ of the raw isotope measurements from the reference value in ~~untils~~ units of ‰ on a ~~delta~~ δ scale for mixing ratio x:

$$\Delta\delta_{corr}(\delta, x) = \delta(x) - \delta_{ref}. \tag{2}$$

440   While Weng et al. (2020) used hyperbolic functions of mixing ratio fitted to measurement points with a set of water standards, we use a new approach that is more flexible in terms of ~~utilizing~~ utilising data points that are mixed from different waters by the microdrop device. To this end, we first remove the dominant first-order dependency on the mixing ratio by a log-transformation of the mixing ratio to $\ln(x)$:

19

$$\Delta\delta_{\mathrm{corr}}(\delta, \ln(x)) = \delta(\ln(x)) - \delta_{\mathrm{ref}}. \tag{3}$$

445   To take all measurements into account, we obtain ~~the reference value~~ δ_{ref} from a 2nd-order polynomial fit to each measurement sequence at a specified isotope ratio. Next, we fit a regular second or third order two-dimensional polynomial to the set of deviations. We find that different ~~analyzers~~ analysers require different polynomials for fitting in the $\Delta\delta$ and the $\ln(x)$ direction. For the four ~~analyzers~~ analysers investigated at FARLAB, a 2nd-order polynomial was sufficient along the $\ln(x)$ axis. Two of the four ~~analyzers~~ analysers had better fitting results with a 3rd-order polynomial in the $\Delta\delta$ direction than with a 2nd-order

450   polynomial. An example for ~~analyzer~~ analyser HIDS2254 shows that the fitted surfaces are to a large degree consistent with the measurement data (Fig. 9).

~~As~~ The 2D polynomial fit is not constrained to zero at the reference level and thus result in an offset at δ_{ref}. Therefore, as a final processing step ~~,~~ to avoid false corrections at reference humidity, we subtract the deviation from zero of the fitted surface at reference humidity along each isotope ratio. Thereby, the RMSE of the correction surface in comparison to the

455   measurement points increases (Table 3). For δ^2H, the RMSE increase is smaller than for δ^{18}O, where the RMSE is very similar to the correction surface of Weng et al. (2020). Despite the different approach compared to Weng et al. (2020), the shape of the correction surface is to first order remarkably consistent with previously published results for the same ~~analyzer~~ analyser (Fig. 10a,b; ~~black and blue lines~~ solid and dashed contours). Compared to measurements, the root-mean square error of the correction obtained in this study is ~~0.82~~ 1.15 ‰ for δ^2H and ~~0.23~~ 0.33 ‰ for δ^{18}O with adjustment for zero at reference

460   mixing ratio (Table 3). At lower mixing ratios, the RMSE is largest, with 1.57 ‰ for δ^2H and 0.43 ‰ for δ^{18}O for the range of 0–5000 ppmv.

Due to the mixing capability of the microdrop device, it is possible to make additional measurements in-between available laboratory standards, and without mixing additional waters beforehand. We also extended the range of the correction to between 5 and -40 ‰ for δ^{18}O and to 10 and -350 ‰ for δ^2H using additional secondary standards. Notably, the microdrop device

465   allows to obtain the data points needed for such a correction function in a semi-automated fashion and with large flexibility. For example, based on this first screening of the dependency for this ~~analyzer~~ analyser, it would be possible to zoom into particularly critical regions ~~og a given analyzer'~~ of a given analyser's dependency function, such as the region with mixing ratios below 2000 ppmv in the δ^{18}O dependency for the current device (Fig. 10b, red shading).

The surface fitting approach presented here also allows to quantify the uncertainty of the surface fits, thus providing access

470   to the contribution from the mixing ratio – isotope ratio correction to the total uncertainty of a final data set. Here, we used a Monte-Carlo approach to determine the standard deviation of the correction values ~~from~~. Thereby, a bootstrap resampling with 50 repetitions was used to draw non-unique samples from the entire dataset. The standard deviation of the 50 realisations ~~of a sub-sample of all available measurements. Standard deviations~~ are largest at the edges of the correction surface, with values of up to 0.6 ‰ for δ^2H (Fig. 10c) and 0.2 ‰ for δ^{18}O (Fig. 10d). Near the center of the correction functions, the uncertainty is

475   much smaller than the correction itself, as constrained by the precision of the sub-sampled microdrop-generated dataset.
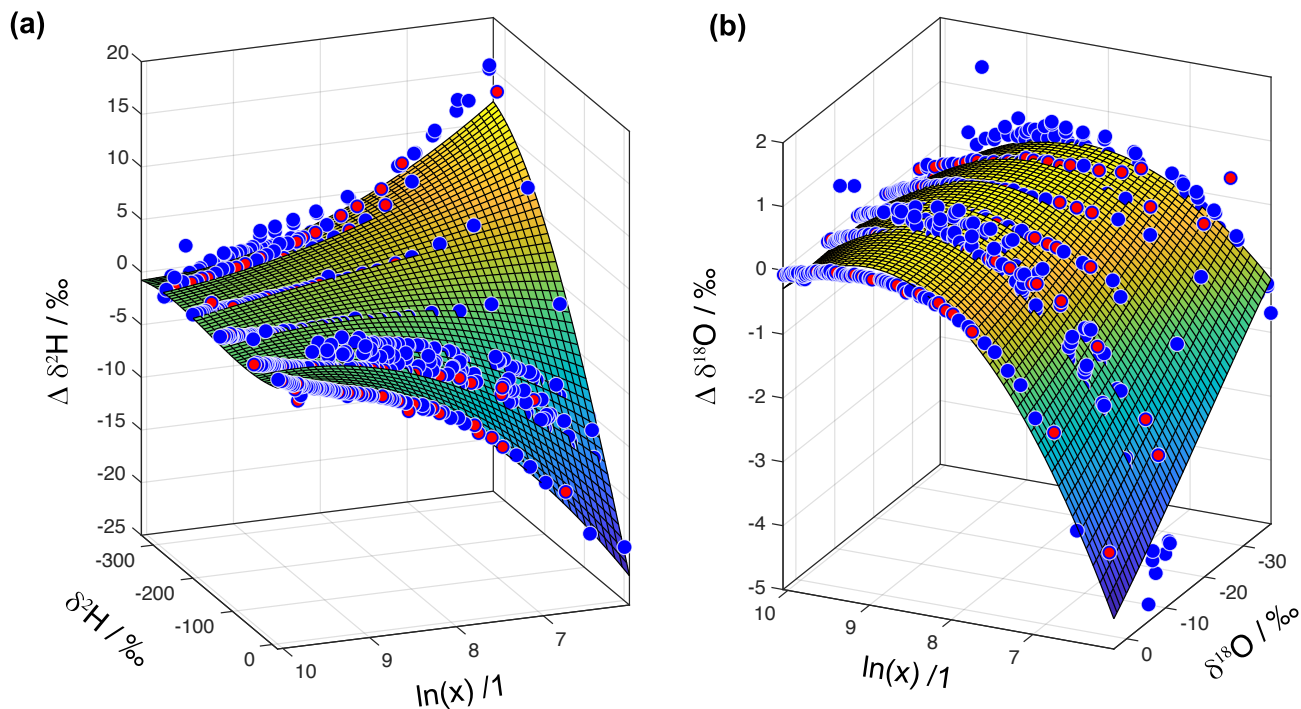
Figure 9. Surface fitting for instrument HIDS2254 for (a) δ^2H and (b) δ^{18}O as a function of ln(mixing ratio). Blue dots show measurement points obtained from microdrop device to constrain the surface fit. Red dots are measurement points obtained from autosampler injections (Weng et al., 2020)

Table 3. Difference between data points obtained from ~~micodrop~~ microdrop measurements and different mixing ratio – isotope ratio correction surfaces, quantified as root-mean square error (RMSE).

| ~~RMSE~~ Method	Mixing ratio range	RMSE δD (‰)	RMSE δ^{18}O (‰)
Weng et al. (2020)	~~1.6630~~ all data	~~0.2276~~ 4.5797	0.4348
polynomial fit	~~0.7009~~ all data	~~0.1780~~ 1.0230	0.2908
polynomial ~~fit with zero adjustment~~ fit*	~~0.8184~~ all data	~~0.2305~~ 1.1514	0.3259
~~for reference mixing ratio~~ polynomial fit*	<5000 ppmv	1.5714	0.4313
polynomial fit*	5000-10'000 ppmv	0.8368	0.2514
polynomial fit*	>10'000 ppmv	0.6441	0.2054

*with zero adjustment for reference mixing ratio
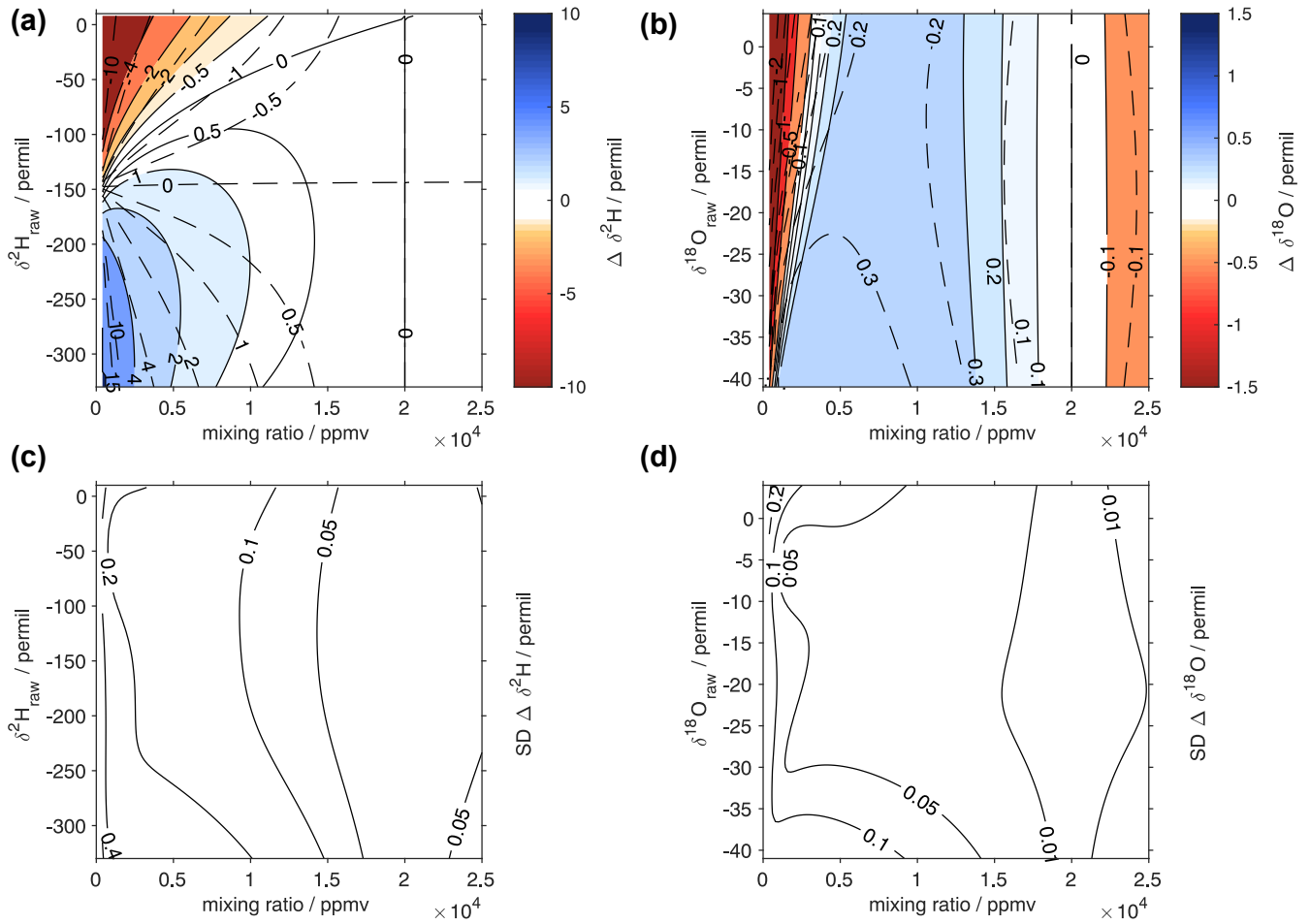
Figure 10. Surface function of the isotopic deviations for (a) $\delta^{18}O$ and (b) δ^2H based on the isotope composition ~~–~~ mixing ratio dependency of Picarro ~~analyzer~~ analyser HIDS2254 (Picarro L2130-i). The horizontal axis is the raw mixing ratio, and the vertical axis shows the raw isotope composition at 20'000 ppmv. ~~Contours~~ Shading and solid contours with numbers indicate the isotopic deviation of ~~$\Delta\delta$~~ $\Delta\delta$. Dashed ~~grey lines~~ contours show the correction functions of Weng et al. (2020). Lower row: standard deviation of correction function obtained from a Monte-Carlo ~~Approach~~ approach (bootstrap resampling) for (c) δ^2H and (d) $\delta^{18}O$ (‰) using 50 random ~~sub-sets~~ non-unique resamplings of the entire dataset.

7 Application 2: $\delta^{18}O$ and δ^2H values of fluid inclusions in stalagmites

We now present an example for an analytical set-up in the laboratory where the microdrop device produces a constant vapour stream with known mixing ratio and isotope composition for fluid inclusion analysis from stalagmites. ~~Voids within the carbonate matrix of stalagmites regularly preserve remnants of cave drip waters. Since these waters are the relics of past~~

480 ~~precipitation, their oxygen and hydrogen isotope compositions can be used to reconstruct past changes in cave temperature (e.g., McGarry et al., 2004; Meckler et al., 2015) and changes in the amount and/or source of precipitation (Fleitmann et al., 2003). Due to the small size of inclusions (<100 μm) and the low amount of water that is commonly present in stalagmites (0.05 to 0.5 weight%; Affolter et al. (2014)), isotope measurements are made on the water that is released when large aliquots (>50 mg) of carbonate are crushed in a heated apparatus. Due to the small water amounts, analysis of fluid inclusions in stalagmites~~

485 ~~requires a background vapour stream with precisely known isotope composition and mixing ratio as carrier gas. This known background enables to separate the superimposed δ^{18}O and δ^2H signals of the water released from calcite cavities during the crushing.~~

~~Measurements have traditionally been obtained with isotope ratio mass spectrometers (IRMS), but these tend to be slow and cumbersome partly due to large memory effects that must be accounted for (e.g., de Graaf et al., 2020). Recent work , however,~~

490 ~~has demonstrated that memory effects can be removed entirely with CDRS techniques if~~ Recently, Affolter et al. (2014) introduced an online method based on CRDS where the water isotope content of fluid inclusions is measured on a standard water background, which is subtracted after peak integration. The result is higher sample throughputs and better reproducibilities than without a moist background (Affolter et al., 2014; Dassié et al., 2018; de Graaf et al., 2020). Recent work indicates that if a moist background is constantly provided to analytical devices (stainless steel lines and ~~crusher devices)are kept under~~

495 ~~humid conditions (Affolter et al., 2014). Fluid inclusion waters are then measured on top of a constant background , which is subtracted after peak integration. The result is higher sample throughputs and better reproducibilities (Affolter et al., 2014; Dassié et al., 201. ~~injection devices), memory effects during the analysis of liquid samples can be substantially reduced (de Graaf et al., 2021).

In all these applications, the precision of the background water vapour and its isotopic composition is critical for the analytical uncertainty of samples. Since the background is subtracted from the sample peak, large variations in the background

500 (mixing ratio and isotopes) are propagated directly into the measured values. de Graaf et al. (2020) argue that even minor instabilities in the background can lead to a loss in measurement precision. Another problem that has been encountered with peristaltic pumps is drift of the background concentration during measurements (Weissbach et al., 2023, their Fig. 2). Here we describe ~~how the micro-dropper device is able to produce a water background of constant isotopic compositions that can be used~~ a setup with the microdrop device for background vapour provision and the corresponding analytical procedures to obtain

505 accurate and precise fluid inclusion δ^{18}O and δ^2H measurements.

7.1 Measurement and data reduction procedures

An analytical line for the sample crushing device (crusher) was built ~~from stainless steel~~ following the design described by Affolter et al. (2014) and de Graaf et al. (2020) (Fig. 11). The upper end is connected to the microdrop device, and the downstream end is connected directly to the ~~analyzer HIDS2254 (~~CRDS analyser (Ser. No. HIDS2254, L2130-i, Picarro Inc)

510 with a union tee fitted with a 1/16 inch capillary as open split. A check valve (Part No. SS-2C-1/3, Swagelok Inc., USA) was installed before the injection port to prevent backflow of sample waters. The injection port consists of a union tee fitted with a rubber septum. The last component is a particle filter (7 μm, Part No. SS-2F-7, Swagelok Inc., USA), which was installed to prevent sample powder from reaching the ~~analyzer~~analyser. All parts of the line are heated to 120 °C with the use of an oven
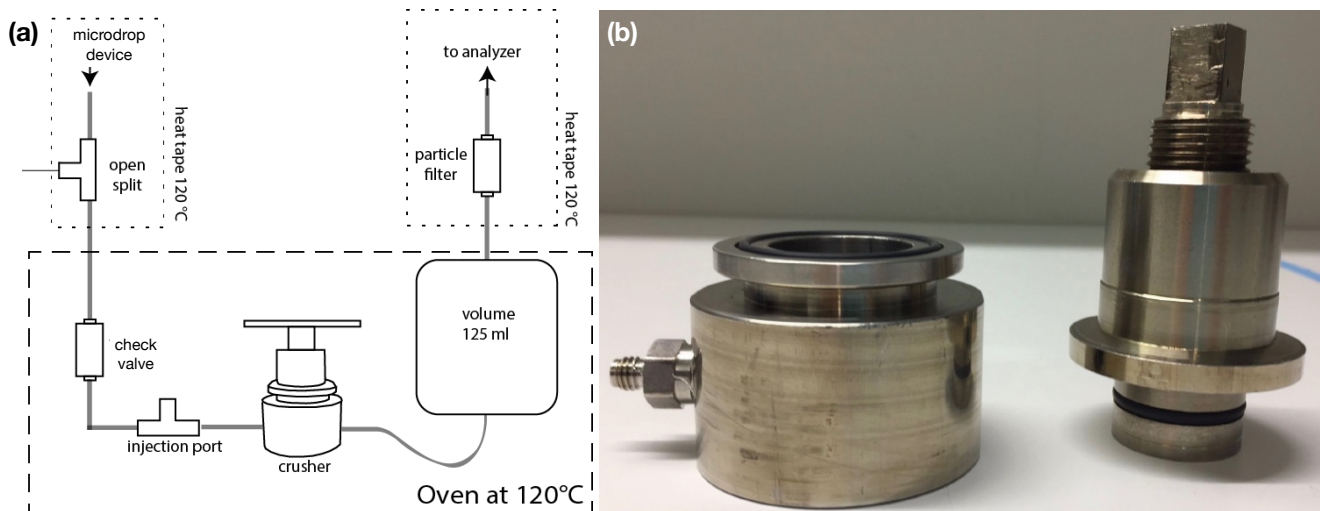
Figure 11. Setup of the crusher system. (a) Schematic of the analytical line for the crusher system. (b) Photograph of the crusher device, built after de Graaf et al. (2020).

(FP 53, Binder GmbH, Germany) or silicon rubber heating tapes (EHG series, Watlow, USA). The crusher is made entirely of

515 stainless steel and ~~it is based on~~ follows the design by de Graaf et al. (2020) with some modifications (Fig. ~~A3~~11). Two Viton O-rings are used to seal the device from atmospheric gases. One ~~ring~~ O-ring is placed on top of the base, and the other is placed on the piston. The piston is threaded to allow up and down movements.

~~Before~~

At the start of an analytical session, the N_2 flow into the microdrop device is set to 90 ~~ssem,~~ sccm, whereby the excess above

520 the ~~flow of~~ 35 sccm used by the ~~analyzer~~ analyser is vented through the open split ~~. The DH~~ (Fig. 11a). The DH frequency is then set to ~~deliver the number of drops per second needed~~ 60–120 Hz to produce a constant mixing ratio of typically 10'000 ~~–~~ 15'000 ppmv~~for frequencies of 60-120 Hz~~, depending on DH efficiency. A sample is subsequently loaded into the crusher (Fig. 11b), and a period of about 20 min is needed for the background H_2O mixing ratio and $\delta^{18}O$ and δ^2H values to ~~stabilize~~ stabilise (Fig. 13, grey area). Once the background is stable, the oven is opened and the thread of the crusher is turned to

525 ~~pulverize~~ pulverise the sample, which causes the fluid inclusions waters to evaporate instantaneously ~~.~~ (Fig. 13, green dot denoted 'start'). During the release of sample water into the background air stream, we note an initial dip to more depleted isotope composition (Fig. 13b,c). Following Affolter et al. (2014), we speculate that this dip stems from kinetic fractionation during the adsorption of water molecules from the background vapour stream onto the newly exposed surface area of the calcite sample. Immediately thereafter, the water peak from the sample arrives on top of the background, here with an enriched

530 signature in the sample. In order to quantify the total water released from the sample, integration is done between start and end of the sample peak (Fig. 13a, dashed black arrow between green dots). Typically, about ~~10-12~~ 10–12 min are needed to measure a complete sample peak.
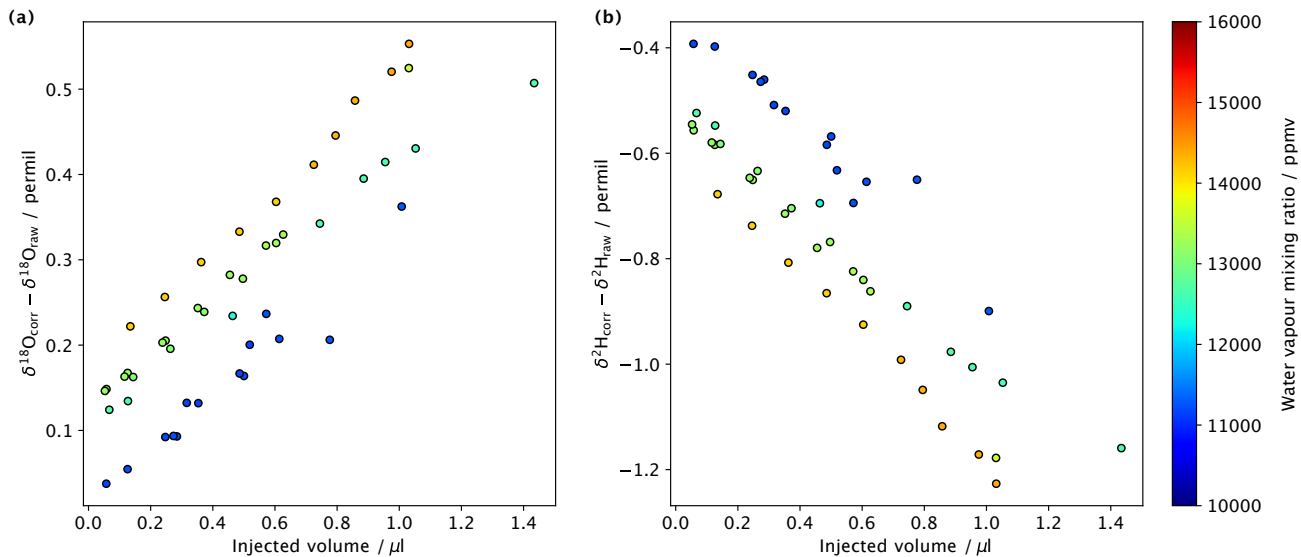
Figure 12. Difference between raw measurements and measurements corrected for spectroscopic baseline effects with the water vapour mixing ratio – isotope ratio dependency from liquid injections of water standard DI in the crushing line on different backgrounds (shading) for (a) δ^2H (permil) and (b) δ^{18}O (permil)

After the water is measured by the ~~analyzer~~ analyser, the data is processed with a series of MATLAB scripts that: (i) correct δ^{18}O and δ^2H values for their humidity dependence (see Sec. 6), (ii) integrate peaks and subtract background values, and

535 (iii) ~~normalize~~ normalise δ^{18}O and δ^2H values to the VSMOW scale and calculate sample H_2O concentrations with standards of known compositions. Mixing ratio – isotope ratio corrections ~~are performed as described in Sec. 6. This is an important step, as the magnitude of the correction depends both on the size of a sample (i.e., amount of water released) and its isotopic composition (Fig. 10). These corrections~~ have not been previously performed in fluid inclusion CDRS data, which may explain why some laboratories observe a ~~size-δ relationship~~ relationship between water amounts and isotope ratio that varies for

540 different standards (e.g., de Graaf et al., 2020). From a sequence of water standard DI2 injected at different amounts and on different water vapour mixing ratios for the background, we see that the mixing ratio – isotope ratio correction clearly translates into measurable signal differences, even when operating not far from the recommended operating range of the analyser (Fig. 12). Some samples with higher water amounts could require even lower background mixing ratios than the 10'000 ppmv applied here, which would lead to an even larger need to correct for spectroscopic baseline effects during peak

545 integration.

~~The next step in the data reduction procedure is to~~

During sample analysis, we integrate the area under the sample ~~peaks~~ peak and subtract the background. This was done following the algorithms described in Affolter et al. (2014). Briefly, raw isotope and H_2O ppmv data (peak and background)

25

are first passed through a running mean filter with a 10 s window to smooth out high frequency variability. The algorithm then finds the start of the peak, which is defined when the rate of change in the water concentration exceeds 5.5 ppmv s^{-1}. Since the rate quickly increases and then turns negative at the top of the peak, the end of the peak is defined after the rate returns to positive values. Next, background values are calculated by averaging values before and after the peak; this was done to account for possible drift in ~~values~~the background isotope composition. After background subtraction, raw sample δ^{18}O and δ^2H values were ~~normalized~~ normalised to the VSMOW scale with three different in-house standards, which were previously calibrated against international standards. For calibration, a range of water amounts (0.05 to $\sim$1.5 μl) were injected with the aid of autosampler GC syringes (0.5 μl SGE Analytical Science and 1 μl Thermo Scientific), and their mean values were used to build a transfer function (Fig. A2). ~~While this step may appear redundant (Sec. 6), it~~ This step ensures that samples and standards receive identical treatments, in particular as the crusher device ~~with~~ can contain calcite remnants and additional components, such as the particle filter ~~can induce different humidity dependencies.~~(Fig. 11). Finally, the amount of water released by the samples was obtained from a transfer function~~constructed with the calculated amounts of water of~~, that had been constructed previously from a series of ~~different samples and the known amounts that were injected~~injections of known amount of standard water.

~~Setup of the crusher system. (a) Schematic of the analytical line for the crusher system. (b) Photograph of the crusher device, built after de Graaf et al. (2020).~~

7.2 Data accuracy and reproducibility

To estimate the reproducibility of our analyses we calculated pooled standard deviations every 0.1 μl (Fig. A3). This was done with the injections used for scale ~~normalization~~normalisation. We observe that standard deviations are very similar for samples larger than 0.3 μl ($<$0.3‰ for δ^{18}O and $<$1.3 ‰ for δ^2H), increase for smaller samples, and are the largest for samples smaller than 0.1 μl (0.7‰ for δ^{18}O and 3.4 ‰ for δ^2H). These reproducibilities are in the range of what has been observed in similar set-ups (Affolter et al., 2014; Dassié et al., 2018; de Graaf et al., 2020).

As a final test of data quality, we measured two samples that have known isotopic compositions. One of the samples consists of 24 aliquots of 0.2 to 0.6 μl of DI standard water that were sealed in borosilicate glass capillaries and crushed in the analytical line (Fig. 14c). Replicates of this sample are designed to mimic real fluid inclusions since, unlike injections, they receive the same treatment (i.e., water is released in the same location by turning the thread of the crusher device; Weissbach (2020)). We find that the mean value of these analyses (δ^{18}O=-7.5$\pm$0.3‰ and δ^2H=-50.9$\pm$1.2‰; $\pm1\sigma$) are statistically indistinguishable from their ~~'known'~~assigned values (Fig. 14a). The second sample (Fig. 14b) is an aliquot of a natural carbonate (Semproniano travertine) that has been previously measured in another laboratory. A total of 4 aliquots of this sample were ~~analyzed~~analysed, and their mean values (δ^{18}O=-4.3$\pm$0.3‰ and δ^2H= -34.3$\pm$1.7‰;$\pm1\sigma$) are statistically indistinguishable from the results obtained by de Graaf et al. (2020) (δ^{18}O=-4.6$\pm$0.32‰ and δ^2H= -33.4$\pm$0.9‰; $\pm1\sigma$, n=4).

In summary, the microdrop vapour generation device enabled a two-fold improvement of the application setup for the measurement of fluid inclusions. First, the characterisation of the ~~analyzer~~analyser allows to correct for the mixing ratio – isotope ratio dependency of the ~~analyzer~~analyser signal, providing a more ~~correct~~accurate integrated signal of each sample than
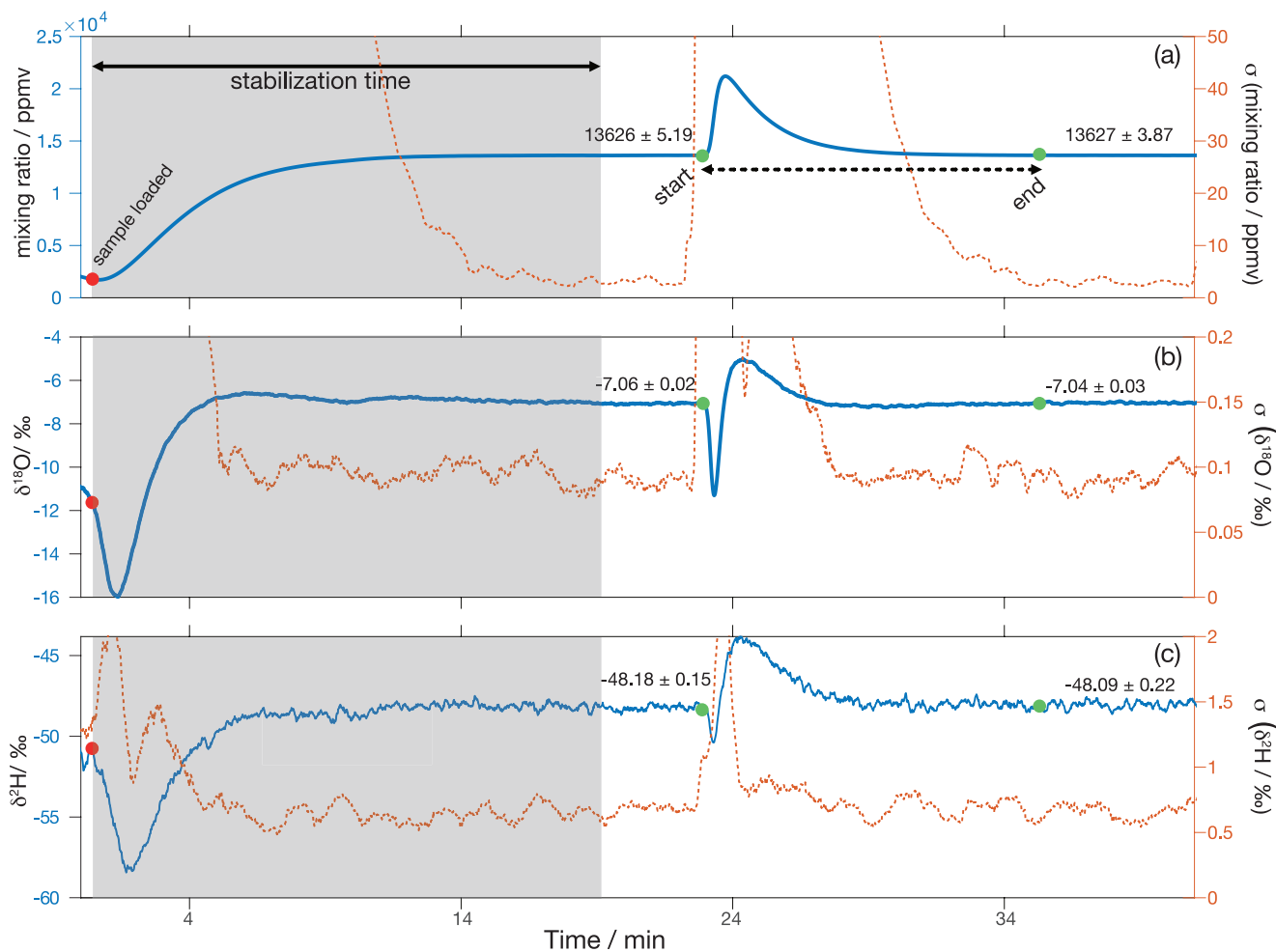
Figure 13. Example of a typical analysis with the crusher and microdrop device. Approximately ~~18-20~~ 18–20 minutes are needed for (a) mixing ratio, and the two water isotope species (b) $\delta^{18}O$ and (c) $\delta^{2}H$ to ~~stabilize~~ stabilise after a sample has been loaded into the crusher device (red circle, ~1 minute). The left axis shows average raw measurements acquired at 0.9 Hz filtered through a 30 s running mean filter, and the right axis shows the standard deviations of the running mean. Background average values before and after the peaks are shown in all panels. Peak values are integrated between the green markers, which show the start and the end of the peak.

without this correction. With the variable water amounts and isotope composition in each sample, and a variable range of set background mixing ratios, this appears as an important additional processing step. Second, the precise background signal of the microdrop device with short-term variance of ~10 ppmv on the time scale of the handling of the crushing device provides a noise-free environment to separate the signal of the fluid inclusion water reliably from the background water stream. In combination, both aspects demonstrate the value of the microdrop technology for specific water isotope measurement applications.
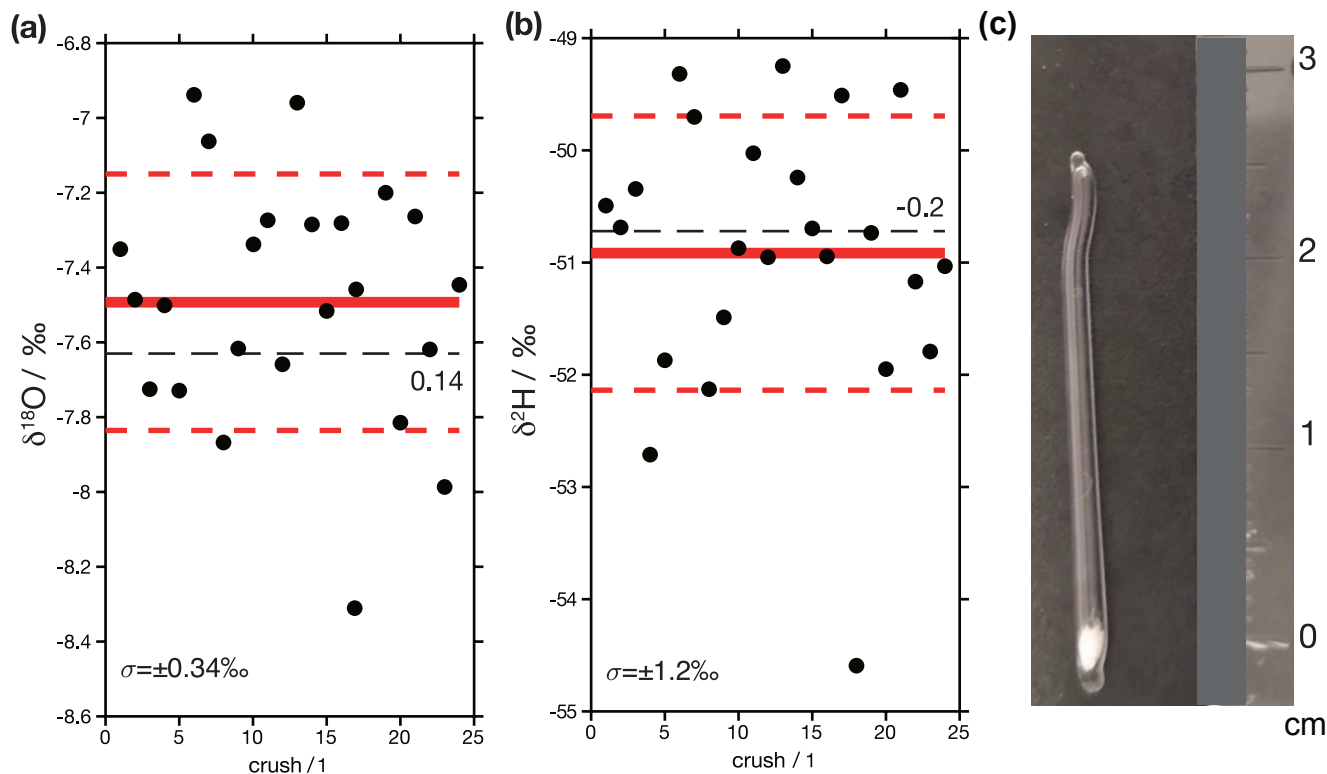
Figure 14. Results from crushed glass capillaries loaded with ~~DI~~ DI2 standard. (a) $\delta^{18}O$ values. The red line shows the mean value of the replicates, and the dashed red lines are the ± 1 standard deviation. The black dashed line is the ~~'true'~~ assigned value of the standard, which is 0.14 ‰ lower than measured mean value. (b) δ^2H values. In this case the ~~'true'~~ assigned value of the standard is 0.2 ‰ higher than the measured mean value. (c) Photograph of a loaded glass capillary. These are built from the capillaries of borosilicate glass pipets. The bottom is sealed and loaded with quartz wool, and water is injected into the wool. The top of the pipet is then sealed. For measurements, the entire pipet is then crushed in the crushing unit.

8   Critical operational aspects and potential error sources

During the operation procedure (Sec. 4), and during operation of one of the application examples (Sec. 6), a number of problems may occur that interrupt or disturb experiments. While in general working reliably over ~~several hours at a time~~hours up to days, these problems are important to be aware of, and one needs to search for remedies in future development of the calibration system.

Potential problems ensue from undetected jets of droplets, that can lead to non-linear or noisy DH characteristics (Sec. 4.2). Finding suitable parameters for single droplet formation, rather than a jet of droplets, is cumbersome and time-consuming process, but should be a rarely repeated procedure for each DH that is ~~utilized. Potential problems ensue from undetected jets of droplets, that can lead to non-linear or noisy DH characteristics (Sec. 4.2).~~ utilised.

During droplet generation, several problems and interruptions can occur. Sturm and Knohl (2010) already reported that the droplet generation stopped occasionally, probably due to formation of bubbles in the injector as the liquid warms up. ~~The procedure involving~~ Therefore, gas removal in an ultrasonic bath and under vaccuum in the headspace (Sec. 4.4, step 2) ~~is intended to prevent such bubbles from forming.~~ before starting dispensing is imperative for reliable dispensing operations. We found that in particular a procedure where vaccuum is briefly applied to the headspace of the liquid makes gas removal dramatically more effective, and prolongs operating times from hours to days.

A further cause for stopping droplet generation can be clogging due to fine particles or residue of salts building up at the dispenser head. While salts can be removed by cleaning procedures, a clogged dispenser head may have to be replaced at some point. Filtering of the standard liquid (Sec. 4.4, step 1) is therefore imperative. While it is conceivable that direct evaporation from the DH capillary may occur at high temperatures and low frequencies, thereby stopping DH operation, more evidence is needed to confirm this potential error source.

A final parameter that could influence DH operation is the holding pressure. The holding pressure is a slight underpressure created by the microdrop controller in the standard vials to prevent liquid from running freely into the evaporation chamber. While typically a holding pressure of about -10 Pa was employed, it could be worth exploring dispensing behaviour for lower holding pressure~~, in particuarly for~~. This is in particularly important for our current design with horizontally mounted DHs~~.~~, where gravitational forces are not aligned with the capillary axis. At higher flow rates, overpressure may build up in the evaporation chamber, which counteracts dispensing by pushing liquid back into the capillary. It may therefore be beneficial to determine the holding pressure relative to the pressure inside the evaporation chamber.

During operation of both dispenser heads, the discrete frequency settings for each DH cause limitations of the mixing ratios between both standard liquids. For example, if both DHs are to contribute no more than 5 drops per second in total, obtaining a partitioning of 1:2 between both heads would require non-integer trigger frequencies, which are currently not allowed by the microdrop controller software. To circumvent this problem, the calibration system can be operated at higher gas flow rates and corresponding higher frequencies, or the controller software needs to be modified.

~~If the calibration system is connected to a downstream application that requires a similar amount of gas flow as the calibration system provides (e.g., a CRDS analyzer operating in high-flow mode), ambient air may enter the analyzer and create an offset in isotope ratio and mixing ratio of the calibration air stream. There are additional aspects that are worth to investigate further, such as~~ A limitation for field operations is the need to refill the calibration standard reservoirs at regular time intervals. The currently used 12 ml vials hold only about 1/4 of the storage bags of the SDM (45 ml). For longer field deployments, a simple modification would be to use larger glass vials with the same thread size as reservoirs for the DHs. In the current design, manual interventions are needed to restart the dispensing heads, preventing unsupervised operation over prolonged time periods.

An important limitation of the ~~change of viscousity of the water due to heating in the cavity, and the build-up of overpressure in the evaporation chamber at~~ current setup is the maximum flow rate of about 250–500 sccm. Even larger flow rates ~~. With active control of such parameters, it can be expected to further increase the precision of the device across a range of~~ would be needed to characterise the response times of entire inlet lines with additional flush pumps used in semi-permanent installations for water isotope analysis (e.g., Steen-Larsen et al., 2013; Bonne et al., 2014; Galewsky et al., 2016). While we have not tested

such an application here, it is technically fairly straightforward to create higher flow rates by diluting the water vapour stream from the microdrop device with dry carrier gas, for example from a gas tank or a dry air generator, or by modifying the tubing, pressure control, gas heating, and dispensing frequency for larger flow rates. Such an extention of the current design, and corresponding characterisation studies are left for future work.

9 Conclusions and implications

Here we describe a new device for the generation of a vapour stream of a specified mixing ratio and water isotope composition based on microdrop dispensing technology. As a key innovation, we operate two dispenser heads in parallel to enable creating a vapour stream with any value along a mixing line between two water standards. We characterise the microdrop vapour generator in terms of the precision of the vapour stream mixing ratio and isotope composition on long and short time scales. Short-term uncertainty of the vapour stream, quantified as Allan deviation, is on the order of 2–10 ppmv for H_2O, up to 0.004 ‰ for $\delta^{18}O$ and about 0.02 ‰ for δ^2H for averaging times of 1000 s. These values are substantially better than a comparable set of measurements obtained with the SDM, which we use as the commercially available benchmark for characterisation of the microdrop device. The long-term precision of 15 min measurement intervals is on the order of 10 ppmv for H_2O, 0.10 ‰ for $\delta^{18}O$, and 0.65 ‰ for δ^2H. These estimates are not substantially affected by either flow rate or dispensing frequency. Simultaneous operation of two dispenser heads provides a linear mixing between two standard waters. The general characteristics of the design in terms of response to flow rate and simultaneous operation of the dispenser heads thus demonstrate that the device functions overall according to specifications set forth in Sec 2.

We use the microdrop vapour generator in two application settings. First, we obtain a semi-automated characterisation of the mixing ratio – isotope ratio dependency for an analyser across a wide range of δ values, more precisely and with lower effort than previously possible. Using a simplified fitting procedure, we obtain a 2-dimensional correction function. Along the $\ln(x)$ axis, a 2nd-order polynomial was sufficient for all four analysers investigated here. Along the $\Delta\delta$ axis, for two of the four analysers a 2nd-order polynomial was sufficient, while the other two had better fitting results with a 3rd-order polynomial. The correction function shows similar overall shape and characteristics for the same analyser over time as in Weng et al. (2020), confirming the stability of this analyser characteristic over months to years. In a second application, we use the microdrop vapour generator in an analytical setup with a crusher device for the analysis of fluid inclusion isotope composition of stalagmite samples. Analysis of standard sample material confirms that the overall analysis works correctly. The high precision of the background humidity from the microdrop vapour generator is a valuable asset in obtaining precise results from the crusher line. Importantly, the availability of a mixing ratio – isotope ratio characterisation for the analyser enables correction of this analyser artefact during peak integration, a factor which has been neglected in previous fluid inclusion studies.

The main advantages of the design are, besides the high precision of the signal, its flexibility in terms of mixing ratio and isotope ratio, absence of moving parts, and low power consumption. Challenges are the occasional stopping due to bubble

665 formation in the dispenser head that requires manual intervention ~~, and the startup procedure~~and makes proper de-gassing of the standard liquid imperative. In addition to a higher degree of automated operation, transfer to a more robust, field-deployable ~~design~~ setup in protective housing would clearly be an advantage over the current prototype version. Nonetheless, our successful demonstration of the overall design has several implications for the water vapour isotope measurements:

(i) The availability of a source of standard vapour that works at different flow rates, mixing ratios, and stable isotope ratios 670 ~~will offer~~ offers a range of possible applications, from regular calibration and instrument or inlet system characterisation, to more ~~specialized operations , involving external equipment.~~ specialised operations as part of an analytical setup in one device. (ii) With the availability of a precise vapour generator, commercial CRDS ~~analyzers~~ analysers can be more commonly ~~corrected for measurement artifacs such as~~ characterized in terms of the mixing ratio – isotope ratio dependency. ~~In addition to analyzer characteristics, the inlet system can influence the measurement signal due to interaction with walls, manifolds, and~~ 675 ~~filters. Tubing to guide ambient vapour to a CRDS analyzer~~, contributing to better data quality of vapour measurements, in particular at low water vapour mixing ratios. (iii) The highly precise continuous stream of water vapour from the microdrop device contributes to lower uncertainty during crushing applications on a moist background gas stream.

One aspect that has not been explored here is the characterisation of inlet lines for water vapour isotope measurements. The inlet tubing can affect the isotope composition~~through memory effects , that result differential retention times at the tubing~~ 680 ~~walls. These effects are dependent on both material, surface structure, and coatings. Prominently, Synflex tubing has been shown to render δ^2H measurements meaningless. Different materials response time to either humidity or isotope composition switches require a stable and well-characterized vapour source. Such effects can be identified and characterised by the provision of~~, for example by memory effects from different materials, depending on flow rates and heating temperatures. Inlet lines could be characterised by providing known pulses of water vapour ~~and water isotopes onto~~ mixing ratio and isotope composition on 685 the inlet system. ~~As a result, signals can either be corrected, or averaged in a suitable way to allow a more reliable separation between geophysical and instrumental signals than is currently possible.~~ This would then enable to optimise the extraction of geophysical signals from measurements. However, substantially larger flow rates of several liters per minute than tested with the current microdrop device are generally required for inlet characterisations. The microdrop device may be able to fill this important gap in water vapour isotope measurements during future follow-up work.

690 *Code and data availability.* The data set and program code are available from the authors on request.

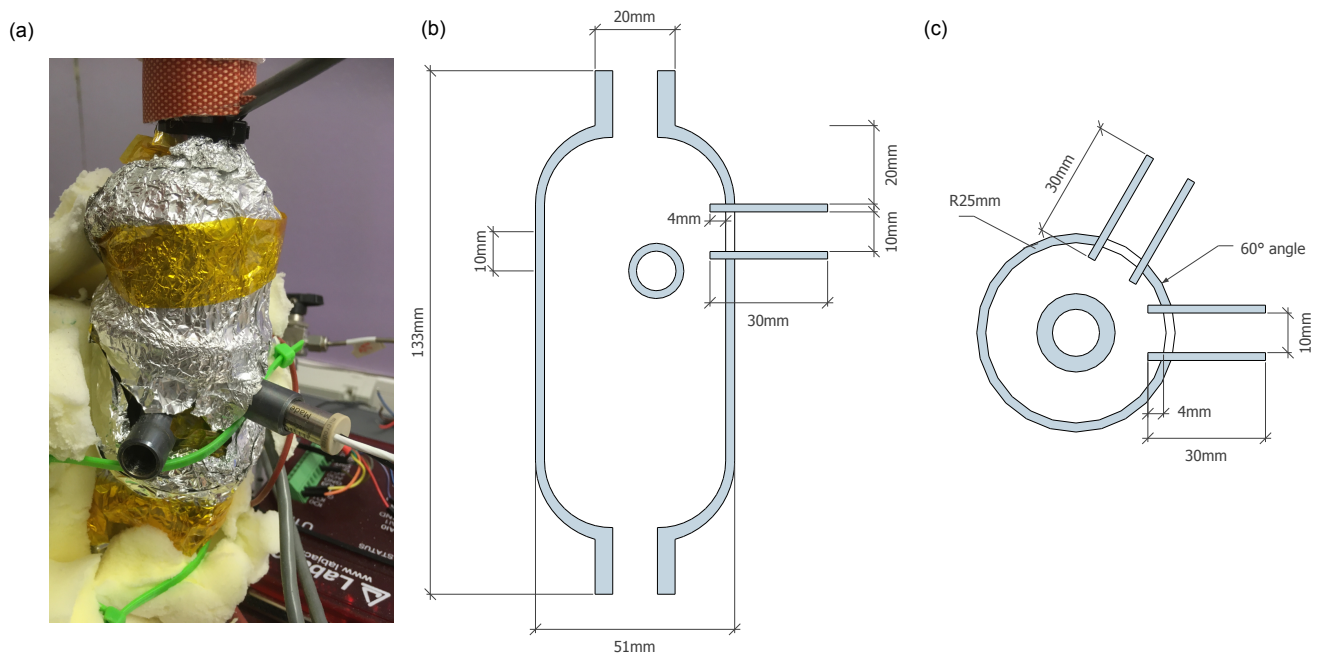**Appendix A: Crusher application details**

31

Figure A1. ~~Sample waters are calibrated~~ Photograph and drawings of the evaporation chamber with ~~three inhouse standards (previously normalized to VSMOW-SLAP)~~dispenser head ports. ~~Panels~~ (~~a-f~~a) ~~show δ^{18}O and δ^{2}H values for injections~~ Photograph of ~~different volumes. Red dashed line are~~ the ~~mean values of~~ dispenser head ports on the ~~standards averaged every 0.1 μl~~evaporation chamber with DH1 inserted. ~~Panels~~ Insulating material has been removed to expose the dispenser head ports. Heat tape is covered by aluminium foil. Plan drawing of (~~g~~b) side view and (~~h~~c) ~~show transfer functions constructed from panels a-f with the mean measured vs~~top view.~~assigned values for δ^{18}O and δ^{2}H.~~
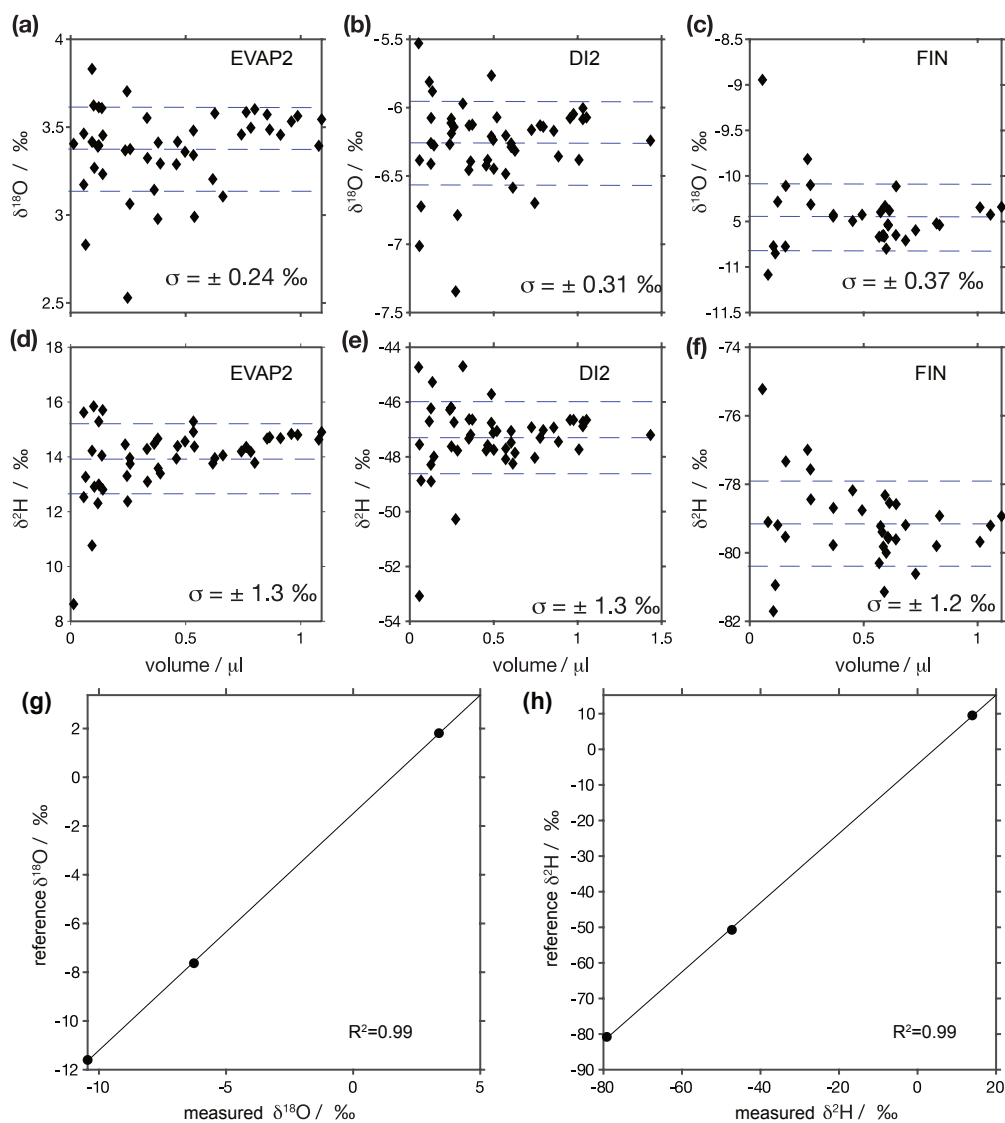
Figure A2. Sample waters are calibrated with three inhouse standards EVAP2 (1.77 ± 0.02 for δ^{18}O; 10.0 ± 0.1 for δ^2H), DI2 (-7.64 ± 0.02 for δ^{18}O; -49.8 ± 0.3 for δ^2H), and FIN (-11.66 ± 0.02 for δ^{18}O; 80.8 ± 0.4 for δ^2H) which have previously been normalised to VSMOW-SLAP scale from liquid injections on CRDS analysers using reference waters obtained from IAEA. Panels (a-f) show δ^{18}O and δ^2H values for injections of different volumes. Dashed lines show the mean values and standard deviation across all water volumes, with 1-σ standard deviation stated in each panel. Panels (g) and (h) show transfer functions constructed from panels a-f with the mean measured vs. assigned values for δ^{18}O and δ^2H. Note that the y-axes differ between panels.
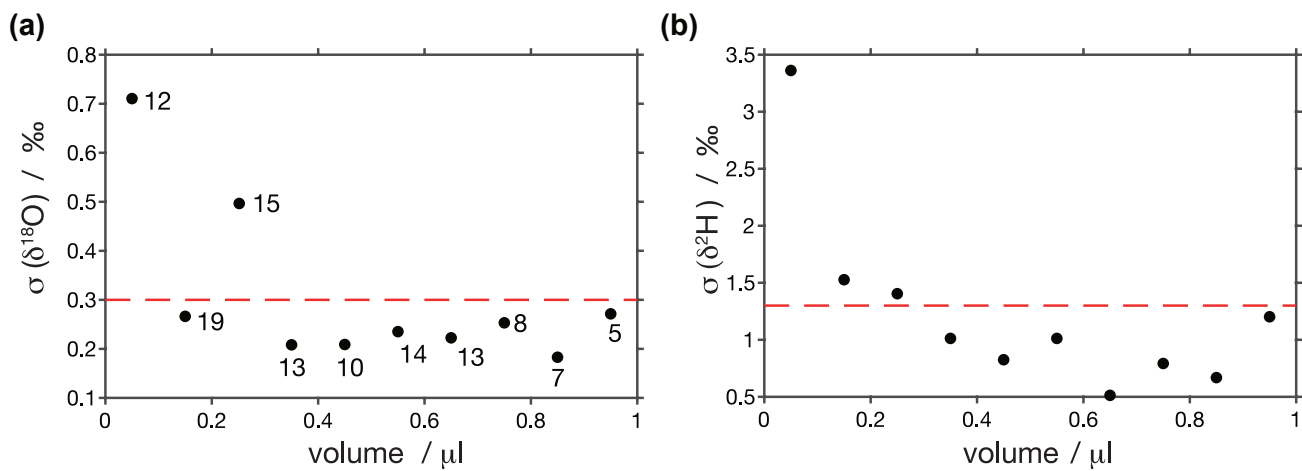
(a)

σ (δ¹⁸O) / ‰ vs volume / µl

(b)

σ (δ²H) / ‰ vs volume / µl

Figure A3. Pooled variance of injections calculated every 0.1 μl. Reproducibilities for samples larger than 0.3 μl are <0.3‰ for (a) δ^{18}O and <1.3 ‰ for (b) δ^2H and increase for smaller samples. Circles are labelled with number of injections used to calculate pooled variance at each point.

Table A1. Date, time, and mixing ratio of the 37 segments used for the short-term stability assessment. Time is the begining of the 15 min interval used to calculate standard deviations in water background and isotope values.

Date	Time	Mean(H_2O)	SD(H_2O)	SD($\delta^{18}O$)	SD(δ^2H)
2020-10-02	12:51:07	11524	29.8	0.133	0.661
2020-10-06	17:02:47	11266	13.6	0.114	0.668
2020-10-09	12:27:45	11193	26.6	0.135	0.673
2020-10-11	15:39:44	11154	10.5	0.098	0.618
2020-10-14	10:51:25	11456	10.6	0.099	0.648
2020-10-14	13:00:50	11444	4.2	0.097	0.647
2020-10-14	14:37:03	11478	4.6	0.091	0.633
2020-10-19	10:14:18	9608	10.3	0.099	0.632
2020-10-19	12:18:44	9558	5.8	0.099	0.630
2020-10-19	13:01:35	9561	3.9	0.097	0.627
2020-10-20	10:37:04	11672	6.5	0.100	0.671
2020-10-20	12:23:13	11640	14.0	0.102	0.662
2020-10-22	13:03:44	12026	10.1	0.096	0.655
2020-10-22	14:30:00	12050	13.1	0.098	0.642
2020-10-23	11:18:42	12079	7.3	0.095	0.644
2020-10-23	12:36:16	12080	9.1	0.097	0.644
2020-10-23	13:44:41	12060	8.5	0.101	0.641
2020-10-27	13:29:00	12064	11.6	0.098	0.653
2020-10-27	17:46:53	12208	8.8	0.099	0.665
2020-10-28	10:19:02	12170	9.7	0.094	0.602
2020-10-28	11:36:25	12092	12.7	0.099	0.644
2020-10-28	14:30:23	11981	10.0	0.102	0.640
2020-10-28	15:28:51	11901	11.8	0.105	0.640
2020-10-30	11:34:02	12286	18.5	0.118	0.661
2020-11-02	11:09:05	12327	11.9	0.098	0.646
2020-11-02	13:57:04	11937	17.9	0.108	0.659
2020-11-02	15:25:24	11928	23.2	0.124	0.668
2020-11-03	11:31:10	11887	24.4	0.130	0.687
2020-11-03	12:09:20	12006	21.8	0.107	0.672
2020-11-06	16:45:40	13346	5.7	0.095	0.674
2020-11-06	17:41:55	13360	6.8	0.099	0.638
2020-11-10	11:52:19	13425	12.5	0.096	0.647
2020-11-10	12:55:17	13390	4.2	0.096	0.643
2020-11-10	17:51:03	13116	6.3	0.092	0.636
2020-11-11	16:40:10	13151	6.7	0.095	0.643
2020-11-11	18:24:41	13053	5.5	0.099	0.674
2020-11-11	19:23:35	13019	8.5	0.098	0.662

References

705 Aemisegger, F., Sturm, P., Graf, P., Sodemann, H., Pfahl, S., Knohl, A., and Wernli, H.: Measuring variations of δ^{18}O and δ^{2}H in atmospheric water vapour using two commercial laser-based spectrometers: an instrument characterisation study, Atmospheric Measurement Techniques, 5, 1491–1511, 2012.

Affolter, S., Fleitmann, D., and Leuenberger, M.: New online method for water isotope analysis of speleothem fluid inclusions using laser absorption spectroscopy (WS-CRDS), Climate of the Past, 10, 1291–1304, 2014.

710 Allan, D. W.: Statistics of atomic frequency standards, Proc. IEEE, pp. 221–230, https://doi.org/10.1109/PROC.1966.4634, 1966.

Bailey, A., Noone, D., Berkelhammer, M., Steen-Larsen, H. C., and Sato, P.: The stability and calibration of water vapor isotope ratio measurements during long-term deployments, Atmospheric Measurement Techniques, 8, 4521–4538, 2015.

Bailey, A., Aemisegger, F., Villiger, L., Los, S. A., Reverdin, G., Quiñones Meléndez, E., Acquistapace, C., Baranowski, D. B., Böck, T., Bony, S., Bordsdorff, T., Coffman, D., de Szoeke, S. P., Diekmann, C. J., Dütsch, M., Ertl, B., Galewsky, J., Henze, D., Makuch, P., Noone,
715 D., Quinn, P. K., Rösch, M., Schneider, A., Schneider, M., Speich, S., Stevens, B., and Thompson, E. J.: Isotopic measurements in water vapor, precipitation, and seawater during EUREC[4]A, Earth System Science Data, 15, 465–495, https://doi.org/10.5194/essd-15-465-2023, 2023.

Bastrikov, V., Steen-Larsen, H. C., Masson-Delmotte, V., Gribanov, K., Cattani, O., Jouzel, J., and Zakharov, V.: Continuous measurements of atmospheric water vapour isotopes in western Siberia (Kourovka), Atmospheric Measurement Techniques, 7, 1763–1776, 2014.

720 Bonne, J. L., Masson-Delmotte, V., Cattani, O., Delmotte, M., Risi, C., Sodemann, H., and Steen-Larsen, H. C.: The isotopic composition of water vapour and precipitation in Ivittuut, southern Greenland, Atmospheric Chemistry and Physics, 14, 4419–4439, 2014.

Bonne, J.-L., Behrens, M., Meyer, H., Kipfstuhl, S., Rabe, B., Schönicke, L., Steen-Larsen, H. C., and Werner, M.: Resolving the controls of water vapour isotopes in the Atlantic sector, Nature Communications, pp. 1–10, 2019.

Casado, M., Landais, A., Masson-Delmotte, V., Genthon, C., Kerstel, E., Kassi, S., Arnaud, L., Picard, G., Prie, F., Cattani, O., Steen-Larsen,
725 H.-C., Vignon, E., and Cermak, P.: Continuous measurements of isotopic composition of water vapour on the East Antarctic Plateau, Atmospheric Chemistry and Physics, 16, 8521–8538, https://doi.org/10.5194/acp-16-8521-2016, 2016.

Dassié, E. P., Genty, D., Noret, A., Mangenot, X., Massault, M., Lebas, N., Duhamel, M., Bonifacie, M., Gasparrini, M., Minster, B., and Michelot, J.-L.: A Newly Designed Analytical Line to Examine Fluid Inclusion Isotopic Compositions in a Variety of Carbonate Samples, Geochemistry, Geophysics, Geosystems, 19, 1107–1122, 2018.

730 de Graaf, S., Vonhof, H. B., Weissbach, T., Wassenburg, J. A., Levy, E. J., Kluge, T., and Haug, G. H.: A comparison of isotope ratio mass spectrometry and cavity ring-down spectroscopy techniques for isotope analysis of fluid inclusion water., Rapid Communications in Mass Spectrometry, 34, e8837, 2020.

de Graaf, S., Vonhof, H. B., Levy, E. J., Markowska, M., and Haug, G. H.: Isotope ratio infrared spectroscopy analysis of water samples without memory effects, Rapid Communications in Mass Spectrometry, 35, e9055, https://doi.org/https://doi.org/10.1002/rcm.9055, 2021.

735 Fernandez, A., Løland, M. H., Maccali, J., Krüger, Y., Vonhof, H. B., Sodemann, H., and Meckler, A. N.: Characterization and Correction of Evaporative Artifacts in Speleothem Fluid Inclusion Isotope Analyses as Applied to a Stalagmite From Borneo, Geochemistry, Geophysics, Geosystems, 24, e2023GC010 857, https://doi.org/https://doi.org/10.1029/2023GC010857, e2023GC010857 2023GC010857, 2023.

Fleitmann, D., Burns, S. J., Neff, U., Mangini, A., and Matter, A.: Changing moisture sources over the last 330,000 years in Northern Oman
740 from fluid-inclusion evidence in speleothems, Quaternary Research, 60, 223–232, 2003.

Galewsky, J., Steen-Larsen, H. C., Field, R. D., Worden, J., Risi, C., and Schneider, M.: Stable isotopes in atmospheric water vapor and applications to the hydrologic cycle, Rev. Geophys., 54, 809–865, 2016.

Gkinis, V., Popp, T. J., Johnsen, S. J., and Blunier, T.: A continuous stream flash evaporator for the calibration of an IR cavity ring-down spectrometer for the isotopic analysis of water, Isotopes In Environmental And Health Studies, 2010.

745 Graf, P., Wernli, H., Pfahl, S., and Sodemann, H.: A new interpretative framework for below-cloud effects on stable water isotopes in vapour and rain, Atmospheric Chemistry and Physics, 19, 747–765, 2019.

Gupta, P., Noone, D., Galewsky, J., Sweeney, C., and Vaughn, B. H.: Demonstration of high-precision continuous measurements of water vapor isotopologues in laboratory and remote field deployments using wavelength-scanned cavity ring-down spectroscopy (WS-CRDS) technology, Rapid Communications in Mass Spectrometry, 23, 2534–2542, 2009.

750 Horita, J., Rozanski, K., and Cohen, S.: Isotope effects in the evaporation of water: a status report of the Craig-Gordon model, Isotopes In Environmental And Health Studies, 44, 23–49, 2008.

Iannone, R. Q., Romanini, D., Kassi, S., Meijer, H. A. J., and Kerstel, E. R. T.: A Microdrop Generator for the Calibration of a Water Vapor Isotope Ratio Spectrometer, Journal Of Atmospheric And Oceanic Technology, 26, 1275–1288, 2009.

Jones, T. R., White, J. W. C., Steig, E. J., Vaughn, B. H., Morris, V., Gkinis, V., Markle, B. R., and Schoenemann, S. W.: Improved
755   methodologies for continuous-flow analysis of stable water isotopes in ice cores, Atmospheric Measurement Techniques, 10, 617–632, https://doi.org/10.5194/amt-10-617-2017, 2017.

Kerstel, E. R. T., Iannone, R. Q., Chenevier, M., Kassi, S., Jost, H. J., and Romanini, D.: A water isotope (H-2, O-17, and O-18) spectrometer based on optical feedback cavity-enhanced absorption for in situ airborne applications, Applied Physics B-Lasers And Optics, 85, 397–406, 2006.

760 Lee, X., Sargent, S., Smith, R., and Tanner, B.: In situ measurement of the water vapor 18O/16O isotope ratio for atmospheric and ecological applications, J. Atmos. Ocean. Techn., 22, 555–565, 2005.

Lis, G., Wassenaar, L. I., and Hendry, M. J.: High-Precision Laser Spectroscopy D/H and 18O/16O Measurements of Microliter Natural Water Samples, Analyt. Chem., 2007.

Maccali, J., Meckler, A. N., Lauritzen, S.-E., Brekken, T., Rokkan, H. A., Fernandez, A., Krüger, Y., Adigun, J., Affolter, S., and Leuenberger,
765   M.: Multi-proxy speleothem-based reconstruction of mid-MIS 3 climate in South Africa, Climate of the Past Discussions, 2023, 1–27, https://doi.org/10.5194/cp-2023-1, 2023.

McGarry, S., Bar-Matthews, M., Matthews, A., Vaks, A., Schilman, B., and Ayalon, A.: Constraints on hydrological and paleotemperature variations in the Eastern Mediterranean region in the last 140 ka given by the δD values of speleothem fluid inclusions, Quaternary Science Reviews, 23, 919–934, 2004.

770 Meckler, A. N., Affolter, S., Dublyansky, Y. V., Science, Y. K. Q., and 2015: Glacial–interglacial temperature change in the tropical West Pacific: A comparison of stalagmite-based paleo-thermometers, Quarternary Science Reviews, 127, 90–116, 2015.

Sayres, D. S., Moyer, E. J., Hanisco, T. F., St Clair, J. M., Keutsch, F. N., O'Brien, A., Allen, N. T., Lapson, L., Demusz, J. N., Rivero, M., Martin, T., Greenberg, M., Tuozzolo, C., Engel, G. S., Kroll, J. H., Paul, J. B., and Anderson, J. G.: A new cavity based absorption instrument for detection of water isotopologues in the upper troposphere and lower stratosphere, Review of Scientific Instruments, 80,
775   044 102–15, 2009.

Seidl, A. W., Sodemann, H., and Steen-Larsen, H. C.: A modular field system for near-surface, vertical profiling of the atmospheric composition in harsh environments using cavity ring-down spectroscopy, Atmospheric Measurement Techniques, 16, 769–790, 2023.

Sodemann, H., Aemisegger, F., Pfahl, S., Bitter, M., Corsmeier, U., Feuerle, T., Graf, P., Hankers, R., Hsiao, G., Schulz, H., Wieser, A., and Wernli, H.: The stable isotopic composition of water vapour above Corsica during the HyMeX SOP1 campaign: insight into vertical mixing processes from lower-tropospheric survey flights, Atmospheric Chemistry and Physics, 17, 6125–6151, 2017.

St Clair, J. M., Hanisco, T. F., Weinstock, E. M., Moyer, E. J., Sayres, D. S., Keutsch, F. N., Kroll, J. H., Demusz, J. N., Allen, N. T., Smith, J. B., Spackman, J. R., and Anderson, J. G.: A new photolysis laser-induced fluorescence instrument for the detection of H2O and HDO in the lower stratosphere., Review of Scientific Instruments, 79, 064 101, 2008.

Steen-Larsen, H. C., Johnsen, S. J., Masson-Delmotte, V., Stenni, B., Risi, C., Sodemann, H., Balslev-Clausen, D., Blunier, T., Dahl-Jensen, D., Ellehøj, M. D., Falourd, S., Grindsted, A., Gkinis, V., Jouzel, J., Popp, T., Sheldon, S., Simonsen, S. B., Sjolte, J., Steffensen, J. P., Sperlich, P., Sveinsbjornsdottir, A., Vinther, B. M., and White, J. W. C.: Continuous monitoring of summer surface water vapor isotopic composition above the Greenland Ice Sheet, Atmospheric Chemistry and Physics, 13, 4815–4828, 2013.

Steig, E. J., Gkinis, V., Schauer, A. J., Schoenemann, S. W., Samek, K., Hoffnagle, J., Dennis, K. J., and Tan, S. M.: Calibrated high-precision ^{17}O-excess measurements using cavity ring-down spectroscopy with laser-current-tuned cavity resonance, Atmospheric Measurement Techniques, 7, 2421–2435, 2014.

Sturm, P. and Knohl, A.: Water vapor δ^{2}H and δ^{18}O measurements using off-axis integrated cavity output spectroscopy, Atmospheric Measurement Techniques, 3, 67–77, 2010.

Thurnherr, I., Kozachek, A., Graf, P., Weng, Y., Bolshiyanov, D., Landwehr, S., Pfahl, S., Schmale, J., Sodemann, H., Steen-Larsen, H. C., Toffoli, A., Wernli, H., and Aemisegger, F.: Meridional and vertical variations of the water vapour isotopic composition in the marine boundary layer over the Atlantic and Southern Ocean, Atmospheric Chemistry and Physics, 20, 5811–5835, https://doi.org/10.5194/acp-20-5811-2020, 2020.

van Geldern, R. and Barth, J. A. C.: Optimization of instrument setup and post-run corrections for oxygen and hydrogen stable isotope measurements of water by isotope ratio infrared spectroscopy (IRIS), Limnology and Oceanography: Methods, 10, 1024–1036, 2012.

Weissbach, T.: Spectroscopic isotope ratio analysis on speleothem fluid inclusions - analytics and paleoclimatic case studies, Ph.D. thesis, University of Heidelberg, 2020.

Weissbach, T., Kluge, T., Affolter, S., Leuenberger, M. C., Vonhof, H., Riechelmann, D. F., Fohlmeister, J., Juhl, M.-C., Hemmer, B., Wu, Y., Warken, S. F., Schmidt, M., Frank, N., and Aeschbach, W.: Constraints for precise and accurate fluid inclusion stable isotope analysis using water-vapour saturated CRDS techniques, Chemical Geology, 617, 121 268, https://doi.org/https://doi.org/10.1016/j.chemgeo.2022.121268, 2023.

Weng, Y., Touzeau, A., and Sodemann, H.: Correcting the impact of the isotope composition on the mixing ratio dependency of water vapour isotope measurements with cavity ring-down spectrometers, Atmospheric Measurement Techniques, 13, 3167–3190, 2020.